

CCL5 promotes breast cancer recurrence through macrophage recruitment in residual tumors

Andrea Walens, Ashley V. DiMarco, Ryan Lupo, Benjamin R. Kroger, Jeffrey S. Damrauer, and James V. Alvarez

Department of Pharmacology and Cancer Biology, Duke University, Durham, NC 27710, USA

Keywords: breast cancer, CCL5, macrophage, collagen

The authors declare that they have no conflict of interest relevant to this work.

ABSTRACT

Over half of breast cancer related deaths are due to recurrence five or more years after initial diagnosis and treatment. This latency suggests that a population of residual tumor cells can survive treatment and persist in a dormant state for many years. The role of the microenvironment in regulating the survival and proliferation of residual cells following therapy remains unexplored. Using a conditional mouse model for Her2-driven breast cancer, we identify interactions between residual tumor cells and their microenvironment as critical for promoting tumor recurrence. Her2 downregulation leads to an inflammatory program driven by $\text{TNF}\alpha/\text{NF}\kappa\text{B}$ signaling, which promotes immune cell infiltration in regressing and residual tumors. The cytokine CCL5 is elevated following Her2 downregulation and remains high in residual tumors. CCL5 promotes tumor recurrence by recruiting CCR5-expressing macrophages, which may contribute to collagen deposition in residual tumors. Blocking this $\text{TNF}\alpha$ -CCL5-macrophage axis may be efficacious in preventing breast cancer recurrence.

INTRODUCTION

In 2018 it is estimated that approximately 270,000 women will be diagnosed with breast cancer, and 41,000 women will succumb to the disease (Siegel et al. 2018). Historically, over half of these deaths are due to recurrence 5 or more years after initial diagnosis and treatment (Sosa et al. 2014). This suggests that in a subset of patients, there is a population of clinically undetectable residual tumor cells that survive therapy, and may serve as a reservoir for eventual relapse. The long latency of recurrence has led to speculation that residual tumor cells are slowly growing or even dormant (Hölzel et al., 2010; Klein, 2009). Understanding how residual cells survive therapy, persist in a non-proliferative state, and eventually resume proliferation to form recurrent tumors is critical for preventing recurrences.

Much of the work examining mechanisms of tumor cell survival and recurrence following therapy has focused on tumor cell-intrinsic pathways (Sosa et al., 2011). Genetic mutations that render cells resistant to therapy represent an important mechanism of survival (Holohan et al., 2013), but there is emerging evidence that non-genetic pathways can also promote survival in response to therapy. For instance, a population of cells called drug-tolerant persisters has been shown to survive therapy through epigenetic adaptations (Sharma et al., 2010). Additionally, epithelial-to-mesenchymal transition has been shown to promote cell survival in response to EGFR inhibitors (Sequist et al., 2011). Finally, alterations in apoptotic pathways within tumor cells can promote cell survival in response to both chemotherapy and targeted therapy (Alvarez et al., 2013; Damrauer et al., 2018; Hata et al., 2016; Holohan et al., 2013; Mabe et al., 2018). In spite of this extensive literature on cell-intrinsic mechanisms of therapeutic resistance, much less is known about tumor cell-extrinsic contributions to cell survival following therapy. Specifically, while there has been some recent focus on how the tumor microenvironment can promote tumor cell survival

in response to therapy (Meads et al., 2009), little is known about whether the microenvironment regulates tumor cell survival, dormancy, and eventual recurrence.

We used a conditional mouse model of Her2-driven breast cancer to examine interactions between tumor cells and their microenvironment during tumor dormancy and recurrence. In this model, administration of doxycycline (dox) to bitransgenic MMTV-rtTA;TetO-Her2/neu (MTB;TAN) mice leads to mammary gland-specific expression of epidermal growth factor receptor 2 (Her2) and the development of Her2-driven tumors. Removal of dox induces Her2 downregulation and tumor regression. However, a small population of residual tumor cells can survive and persist in a non-proliferative state (Alvarez et al., 2013; Moody, 2002). These cells eventually re-initiate proliferation to form recurrent tumors that are independent of Her2. Using this model, we sought to understand how the interplay between tumor cells and their microenvironment regulates residual cell survival and recurrence.

RESULTS

Her2 downregulation induces an inflammatory gene expression program driven by the TNF α /IKK pathway

To understand how interactions between tumor cells and their environment change in response to therapy, we first examined gene expression changes following Her2 downregulation in Her2-driven tumor cells. Two independent cell lines derived from primary Her2-driven tumors (Alvarez et al., 2013; Moody, 2002) were cultured in the presence of dox to maintain Her2 expression, or removed from dox for 2 days to turn off Her2 expression. Changes in Her2 expression following dox withdrawal were confirmed by qPCR analysis (Figure 1 – figure supplement 1A). Changes in gene expression were measured by RNA sequencing. Her2 downregulation led to widespread changes in gene expression in both cell lines (Figure 1A). Gene set enrichment analysis showed that an E2F signature was the most highly enriched gene set in cells with Her2 signaling on (+dox; Figure 1 – figure supplement 1B), consistent with previous literature and the observation that Her2 is required for the proliferation of these cells (Lee et al., 2000). Interestingly, the gene sets most significantly enriched in cells following Her2 downregulation (-dox) were an inflammatory gene signature and a TNF α /NF κ B gene signature (Figure 1B). These gene sets comprised genes encoding chemokines in the CCL family (CCL2, CCL5, and CCL20) and CXCL family (CXCL1, CXCL2, CXCL3, CXCL5, and CXCL10), proteins that mediate cell-cell interactions (TLR2, ICAM1, and CSF1) as well as signaling components of the NF κ B pathway (NFKBIA and NFKBIE). All of these genes were upregulated following Her2 downregulation (Figure 1C).

At high concentrations (>40 μ g/ml) doxycycline itself can inhibit the NF κ B pathway (Alexander-Savino et al., 2016; Santa-Cecília et al., 2016). Although the concentrations of dox (2

μg/ml) we use to culture primary tumor cells are well below these levels, we wanted to confirmed that the NFκB pathway activation observed following dox withdrawal was due to loss of Her2 signaling. To do this, we treated primary tumor cells with Neratinib, a small-molecule inhibitor of Her2, to inhibit Her2 signaling without removal of dox. Neratinib treatment led to an increase in phospho-p65 (Figure 1 – figure supplement 1C), increased expression of TNFα (Figure 1 – figure supplement 1D), and increased expression of the NFκB targets CXCL5 and CCL5 (Figure 1 – figure supplement 1E and F). To further confirm that the low concentrations of dox used to culture primary tumor cells do not directly inhibit the NFκB pathway we treated NIH3T3 cells with TNFα in the presence or absence of 2 μg/ml dox and measured NFκB target genes. Dox treatment had no effect on the induction of NFκB target genes following TNFα treatment (Figure 1 – figure supplement 1G). Taken together, these results demonstrate that Her2 inhibition leads to activation of the NFκB pathway.

Given the coordinated upregulation of these NFκB target genes, we reasoned that their expression may be induced by a common upstream secreted factor acting in an autocrine manner. To test this, we collected conditioned media from primary tumor cells grown in the absence of dox for 2 days. This conditioned media was supplemented with dox to maintain Her2 expression and added to naïve primary tumor cells. Treatment with conditioned media led to a time-dependent upregulation of the pro-inflammatory chemokine CCL5 (Figure 1D). One common upstream mediator of this cytokine response is tumor necrosis factor alpha (TNFα), and we found that TNFα expression is increased between 10-fold and 100-fold following Her2 downregulation (Figure 1E). To test whether this is sufficient to activate downstream signaling pathways, we examined activation of the NFκB pathway following treatment with conditioned media from cells following Her2 downregulation. Indeed, we found that treatment of naïve cells with Her2-off (–dox)

conditioned media led to rapid, robust, and prolonged activation of the NF κ B pathway as assessed by phosphorylation of p65 (Figure 1F). Importantly, Her2 levels remained high in these target cells (Figure 1 – figure supplement 1H), indicating that Her2-off (–dox) conditioned media can activate the NF κ B pathway even in the presence of Her2 signaling. In contrast, conditioned media from Her2-on (+dox) cells had no effect on p65 phosphorylation (Figure 1 – figure supplement 1I). Finally, we tested whether the induction of chemokine genes following Her2 downregulation was dependent upon the NF κ B pathway by treating cells with the IKK inhibitor, IKK16. We found that blocking IKK activity blunted the induction of all chemokine genes following dox withdrawal (Figure 1G). Taken together, these results suggest that Her2 downregulation leads to the induction of a pro-inflammatory gene expression program, likely driven by autocrine-acting TNF α and mediated through the IKK-NF κ B pathway.

Immune cell infiltration during tumor regression and residual disease

Her2 downregulation in Her2-driven tumors *in vivo* induces apoptosis and growth arrest, ultimately leading to tumor regression (Moody, 2002). However, a small population of tumor cells can survive Her2 downregulation and persist for up to 6 months before resuming growth to form recurrent tumors. These residual tumors can be identified histologically (Figure 2A). Many of the cytokines and chemokines induced shortly after Her2 downregulation function as chemoattractants for various immune cells (Binnewies et al., 2018; López et al., 2017). This led us to speculate that Her2 downregulation *in vivo* may promote infiltration of immune cells into the tumor. We therefore asked whether the immune cell composition of tumors changed during tumor regression and in residual tumors. CD45 staining showed that leukocyte infiltration increased dramatically following Her2 downregulation as compared to primary tumors (Figure 2B-C, Figure 2 – figure supplement 1A). Surprisingly, leukocytes remained high in residual tumors (Figure 2D, Figure 2

– figure supplement 1A). Masson’s trichrome staining revealed prominent collagen deposition in residual tumors (Figure 2D), consistent with a desmoplastic response in residual tumors. Staining for the macrophage marker F4/80 showed a dramatic increase in macrophage abundance during tumor regression (Figure 2C, Figure 2 – figure supplement 1A), and macrophage levels remained elevated in residual tumors (Figure 2D, Figure 2 – figure supplement 1A). CD3 staining showed increased T cell infiltration in regressing and residual tumors (Figure 2 – figure supplement 1A,B). Taken together, these results indicate that Her2 downregulation leads to the infiltration of CD45+ leukocytes, and specifically F4/80+ macrophages. Residual tumors contain high numbers of macrophages and abundant collagen deposition, consistent with a desmoplastic response.

Cytokine profiling of residual tumors

Immune cells can influence tumor cell survival and function (Flores-Borja et al., 2016; Pollard, 2004). The large number of immune cells present in residual tumors suggests that these cells may function to regulate the behavior of residual tumor cells. To begin to address this, we sought to identify secreted factors that are expressed in residual tumors. Residual tumor cells in the autochthonous MTB;TAN model are unlabeled and are diffusely scattered throughout the mammary gland, precluding their isolation. Therefore, we used an orthotopic model in which residual tumors can be easily isolated. In this model, primary Her2-driven tumors are digested, cultured, and infected with GFP. Cells are then injected into the mammary fat pad of recipient mice on dox to generate an orthotopic primary tumor. Following dox withdrawal, the fluorescently labeled residual tumors can be easily microdissected (Figure 2 – figure supplement 1C). We first confirmed that the orthotopic model exhibited similar patterns of immune cell infiltration as the autochthonous model. Indeed, we found that macrophage staining increased dramatically during

tumor regression and in residual tumors (Figure 2 – figure supplement 1D-F), suggesting the orthotopic model is appropriate for identifying secreted proteins present in these residual tumors.

We generated a cohort of orthotopic primary tumors (n=4) and residual tumors at 28 days (n=6) and 56 days (n=6) following dox withdrawal. Residual tumors were microdissected using a fluorescent dissecting microscope. We then made protein lysates from all samples and measured the expression of cytokines and chemokines using antibody-based protein arrays. Four primary tumors and four 28-day residual tumors were profiled using a commercially available cytokine array, which measures the expression of 20 secreted factors. We then used a second commercially available cytokine array, which measures 40 cytokines and chemokines, to measure cytokine expression in the whole cohort of tumors. This analysis identified 8 cytokines that were upregulated in residual tumors as compared to primary tumors (Figure 3A; fold change >2, p<0.1, Figure 3 – source data), including CCL5, osteoprotegerin (OPG), and Vascular cell adhesion protein 1 (VCAM-1) (Figure 3B). Interestingly, VCAM-1 has been shown to regulate breast cancer dormancy (Lu et al., 2011), while OPG can regulate the survival of breast cancer cells (Neville-Webbe et al., 2004).

We next asked whether any cytokines were both induced acutely following Her2 downregulation and remained elevated in residual tumors. We found that only two cytokines, CCL5 and OPG, fulfilled these criteria. Given that OPG has previously been associated with dormancy, we focused our attention on CCL5. We then wanted to determine if CCL5 expression was elevated in human residual breast tumors following treatment. We analyzed a gene expression dataset of residual breast tumors that remain following neoadjuvant targeted therapy. A number of secreted factors were upregulated in residual tumors as compared to primary tumors, and CCL5 was one of the most significantly upregulated cytokines in this group (Figure 3C-D and Figure 3

– figure supplement 1A-M). To confirm these results, we examined an independent gene expression data set from breast cancer patients treated with neoadjuvant chemotherapy. We found that CCL5 expression was also increased in residual tumors in this dataset (Figure 3 – figure supplement 1N). These results suggest that CCL5 upregulation is a common feature of residual tumors cells that survive both conventional and targeted therapy in mice and humans, suggesting it may be functionally important in mediating the survival of these cells.

CCL5 expression promotes recurrence following Her2 downregulation

We next wanted to directly assess whether CCL5 plays a functional role in regulating residual cell survival or recurrence. We first used an ELISA to measure CCL5 levels in orthotopic primary tumors, residual tumors, and recurrent tumors. CCL5 expression was elevated in residual tumors, confirming results from the cytokine array, and increased further in recurrent tumors (Figure 4A). We next engineered primary tumor cells to overexpress CCL5 or GFP as a control (Figure 4B) and used these cells in an orthotopic recurrence assay to test the effect of CCL5 expression on tumor recurrence. Control or CCL5-expressing cells were injected orthotopically into recipient mice on doxycycline to maintain Her2 expression. Primary tumors formed with similar kinetics following injection of control and CCL5-expressing cells, indicating that CCL5 expression had no effect on the growth of primary tumors (data not shown). Following primary tumor formation, mice were removed from dox to induce Her2 downregulation and tumor regression. Mice with residual tumors were palpated biweekly to monitor the formation of recurrent tumors. Tumors expressing CCL5 recurred significantly earlier than control tumors, indicating that CCL5 expression is sufficient to accelerate tumor recurrence (Figure 4C; $p=0.023$; HR=2.14).

We next asked if tumor-derived CCL5 is necessary for recurrence. To this end, we used CRISPR-Cas9 to knock out CCL5 in primary tumor cells (Figure 4D), and tested the effect of CCL5 knockout on recurrence using the orthotopic recurrence assay described above. The growth of CCL5 knockout tumors was not different from control tumors expressing a non-targeting sgRNA (data not shown). Mice were removed from dox, and the latency of recurrence between control and CCL5 knockout tumors was compared. We found that CCL5 knockout had no effect on the latency of recurrence (Figure 4E). Taken together, these results suggest that CCL5 expression is sufficient to accelerate recurrence, but tumor-derived CCL5 is not necessary for recurrence following Her2 downregulation.

CCL5 promotes macrophage infiltration in residual tumors

CCL5 is a chemoattractant for various cell types, including T cells, B cells, eosinophils, basophils, neutrophils, macrophages, and fibroblasts (Dembic, 2015; Lacy, 2017; Lee et al., 2017). We observe an increase in CCL5 levels during tumor regression and in residual tumors that is concomitant with immune cell infiltration. We therefore reasoned that the effect of CCL5 overexpression on recurrence may be mediated through its ability to recruit one or more of these cell types to residual lesions and recurrent tumors. CCL5 can signal through multiple receptors, including CCR1, CCR3, and CCR5, but it predominately acts through CCR5 (Soria and Ben-Baruch, 2008). We therefore examined CCR5 expression on various immune and stromal cells in primary tumors (+dox), regressing tumors (5 days -dox), residual tumors (69 days -dox), and recurrent tumors by flow cytometry. As expected, Her2 was downregulated following dox withdrawal in all tumors (Figure 5 – figure supplement 1A). For each cell type, we measured the median fluorescence intensity (MFI) of CCR5 staining in CCR5+ cells. Interestingly, the level of

CCR5 expressed on macrophages increased in residual tumors (Figure 5A and Figure 5 – figure supplement 2). In contrast, CCR5 expression on CD4⁺ T cells CD8⁺ T cells increased in regressing tumors, but returned to baseline in residual tumors (Figure 5B and C, Figure 5 – figure supplement 2). Similar to macrophages, the expression of CCR5 on fibroblasts was elevated in residual tumors (Figure 5D, Figure 5 – figure supplement 2). We were also interested in examining CCR5 expression on CD45⁺ tumor cells. We observed a slight increase in CCR5 expression in residual tumor cells, but otherwise there was no change in CCR5 expression on these cells (Figure 5E). To directly compare the expression of CCR5 in macrophages and tumor cells, we sorted these two populations from primary, regressing, residual, and recurrent tumors from MTB;TAN mice and performed qPCR analysis. CCR5 was expressed at higher levels on macrophages than tumor cells at each stage, and its expression was especially high on residual tumor macrophages (Figure 5 – figure supplement 1B). Overall, these results identify several cell types – notably macrophages and fibroblasts – that express high levels of CCR5 and so are poised to respond to CCL5 in residual tumors.

To determine whether these cell types are recruited by CCL5 in residual tumors, we generated primary and residual tumors overexpressing CCL5 and analyzed the abundance of macrophages and fibroblasts by flow cytometry. Fibroblast levels were not significantly different between control and CCL5-expressing tumors (Figure 5F, Figure 5 – figure supplement 1C). In contrast, CCL5-expressing tumors exhibited a modest but consistent increase in macrophage infiltration (Figure 5G, Figure 5 – figure supplement 1D). Taken together, these results suggest that CCL5 expression in residual tumors can recruit CCR5-positive macrophages, and suggest that CCL5 may subsequently signal through CCR5 on these cells to modulate macrophage function.

Macrophages express and secrete collagen and collagen deposition factors

We next considered the possibility that CCL5 recruitment of macrophages to residual tumors may promote recurrence through macrophage-tumor cell crosstalk. To address this, we sorted CD45+/CD11b+/F4/80+ macrophages from primary, residual and recurrent tumors from the autochthonous MTB;TAN model by fluorescence activated cell sorting (FACS), and then isolated RNA from the sorted cell populations for RNAseq. Residual tumor-associated macrophages did not yield sufficient RNA for RNAseq, but we were able to sequence RNA from primary, regressing, and recurrent tumor-associated macrophages (TAMs). Examination of differentially expressed genes between primary and recurrent TAMs suggested that FACS-sorted TAMs may have been partially contaminated with tumor cells. For instance, we detected Her2 expression at high levels in primary TAMs and low levels in recurrent TAMs. Therefore, we used a gene expression dataset of primary and recurrent tumor cells cultured in vitro to filter the TAM expression list (Figure 6 – source data 1). After filtering, we were left with approximately 200 genes that were differentially expressed between primary and recurrent tumor macrophages (Figure 6A, Figure 6 – source data 2). Interestingly, genes encoding fibrillar collagen and collagen deposition proteins were more highly expressed in the recurrent TAMs than the primary TAMs or regressing tumor TAMs (Figure 6B). These genes include Collagen alpha-1(V) chain (COL5A1), Collagen type XXIV alpha 1 (COL24A1), Procollagen C-endopeptidase enhancer 1 (PCOLCE), and Asporin (ASPN). COL5A1 and COL24A1 encode fibrillar collagens, PCOLCE encodes a glycoprotein that binds and drives the cleavage of type 1 fibrillar procollagen, and ASPN encodes a protein that binds to fibrillar collagens to regulate mineralization. We next sought to validate these findings by performing qPCR analysis on primary, regressing, residual, and recurrent TAMs. This analysis showed that the expression of these genes progressively increased during tumor regression, residual disease, and recurrence (Figure 6C). Additionally, qPCR on RNA isolated

from bulk tumors showed higher expression of COL5A1 and COL24A1 in recurrent tumors, while a subset of recurrent tumors had high expression of ASPN and PCOLCE (Figure 6D). Consistent with this, Masson's trichrome staining showed increased collagen deposition in residual and recurrent tumors (Figure 6E, middle and bottom). In order to see if similar gene expression patterns are observed in residual disease in breast cancer patients, we examined gene expression data from residual tumors after neoadjuvant targeted therapy. Indeed, expression of these four collagen genes increased in residual tumors following therapy (Figure 6 – figure supplement 1A). Finally, we asked whether CCL5 regulates collagen deposition by comparing collagen levels in control and CCL5-expressing recurrent tumors. While control recurrent tumors had uniform levels of collagen deposition (Figure 6F and Figure 6 – figure supplement 1B-C), a subset of CCL5-expressing tumors had very high levels of collagen deposition (Figure 6F and Figure 6 – figure supplement 1B-C). Taken together, these results suggest that CCL5 promotes macrophage infiltration and collagen deposition. Given the importance of collagen for regulating tumor cell function, this may be one mechanism by which CCL5 expression accelerates recurrence. This is reminiscent of findings in colorectal cancer, where collagen deposition can be mediated in part through CCR2+ macrophages, and depletion of these macrophages inhibits tumor growth (Afik et al., 2016).

DISCUSSION

The long-term survival of residual tumor cells following therapy is a major obstacle to obtaining cures in breast cancer. Understanding the pathways that promote residual cell survival – and that induce the reactivation of these cells to generate recurrent tumors – is critical for designing therapies to prevent breast cancer relapse. There has been extensive focus on tumor cell-intrinsic pathways that allow cells to survive therapy (Holohan et al., 2013). However, the role of tumor

cell-extrinsic factors, including the tumor microenvironment, in regulating the survival and recurrence of residual cells has not been extensively explored.

Here we used a conditional mouse model to investigate how interactions between tumor cells and the tumor microenvironment change during tumor regression, residual disease, and recurrence, and in turn how the microenvironment regulates tumor recurrence. We found that Her2 downregulation led to induction of a pro-inflammatory gene expression program comprising a number of chemokines and cytokines, including CCL5. This program was mediated by autocrine TNF α and dependent upon IKK/NF κ B signaling. Notably, a recent study identified a similar gene expression program in EGFR-mutant lung cancer following treatment with EGFR inhibitors (Gong et al., 2018). Consistent with this pro-inflammatory gene expression program, we observed differences in immune and stromal cell infiltration during tumor regression. Both adaptive (CD4⁺ and CD8⁺ T cells) and innate (macrophages) immune cells were recruited to regressing tumors. The residual tumor microenvironment is markedly different from that of primary tumors, with high numbers of macrophages and fibroblasts, abundant collagen deposition, and differential expression of a suite of cytokines, including CCL5. Functionally, CCL5 overexpression promotes macrophage recruitment, collagen deposition, and promotes tumor recurrence. These results identify CCL5 as a critical regulator of crosstalk between residual tumor cells and the residual tumor microenvironment that promotes tumor recurrence.

A number of studies have found that Her2 signaling directly activates the NF κ B pathway, and that this is functionally important for tumor growth (Liu et al., 2009). Consistent with this, we observed basal levels of p65 phosphorylation in primary tumor cells. Surprisingly, we found that Her2 inhibition further activates the NF κ B pathway, and that this occurs through an autocrine pathway that is likely mediated by increased TNF α expression. Hyperactivation of the NF κ B

pathway in turn leads to the production of a number of cytokines and chemokines which may contribute to the recruitment of immune cells. These findings are consistent with prior work showing that the NF κ B pathway is required for macrophage recruitment in a similar Her2-driven mouse model (Liu et al., 2010). Our findings add to these previous studies by showing that Her2 inhibition leads to hyperactivation of the NF κ B pathway and increased macrophage recruitment.

CCL5 has been shown to play an important role in many facets of tumor progression, such as invasion, metastasis, neoangiogenesis, and immune cell infiltration (Aldinucci and Colombatti, 2014). In glioblastoma, CCL5 upregulation has been correlated with recurrence in post-treatment tumors (Hudson et al., 2018). In triple-negative breast cancer, CCL5 expression has also been correlated with residual tumor size and tumor infiltrating lymphocytes after neoadjuvant chemotherapy (Araujo et al., 2018). However, CCL5 has not previously been implicated in residual cell survival or recurrence in Her2+ or hormone receptor positive breast cancer. By analyzing gene expression datasets from breast cancer patients treated with neoadjuvant targeted or chemotherapy (Creighton et al., 2009; Tempfer, 2011), we show here that CCL5 expression is elevated in residual tumor cells that survive therapy. A notable observation in our study is that while CCL5 expression promoted recurrence (Figure 4C), knockout of CCL5 in tumor cells did not delay recurrence (Figure 4E). This suggests that CCL5 may be at least partially redundant with other chemokines, such as CCL2 and CXCL1 and 2, in recruiting macrophages to promote recurrence.

Mechanistically, we show that CCL5 acts to recruit CCR5+ macrophages to residual tumors, consistent with its known role as a chemoattractant factor for macrophages (Mantovani et al. 2017). RNAseq analysis of primary and recurrent TAMs suggested that recurrent TAMs have high expression of genes encoding fibrillar collagen and proteins required for collagen deposition. qPCR analysis indicated that residual TAMs shared this gene expression program. Consistent with

this, collagen deposition is high in residual and recurrent tumors, and CCL5 expression promotes collagen deposition. Collagen deposition is traditionally thought to be driven by fibroblasts in the microenvironment (Thannickal, 2012). However, a recent report showed that macrophages are responsible for collagen deposition in a mouse model of colorectal cancer (Afik et al., 2016). Collagen deposition is important for tumor progression and invasiveness (Provenzano et al., 2008). Collagen bundles can potentiate cell migration and increase tissue stiffness, and enzymes which crosslink collagens are often upregulated in breast cancer and are correlated with a poor prognosis (Lu et al., 2012). It is possible that collagen deposition may promote the survival or proliferation of residual tumor cells, and that this mediates the effect of CCL5 on tumor recurrence.

The findings reported here suggest that efforts to block CCL5-driven macrophage infiltration and subsequent collagen deposition may have therapeutic benefit. Possible therapies include the use of Maraviroc, a CCR5 antagonist (Velasco-Velazquez et al., 2012), and agents that block macrophage infiltration or function, such as the CSF-1R inhibitor PLX3397 (DeNardo et al., 2011; Strachan et al., 2014; Zhu et al., 2014). It is also possible that, because CCL5 is sufficient but not necessary for tumor recurrence, it would be preferable to block the induction of the pro-inflammatory program that is induced following Her2 downregulation using agents targeting TNF α or the NF κ B pathway.

It is important to note that while our studies focus on the function of CCL5 in recruiting CCR5+ macrophages, breast cancer cells themselves can also express CCR5. Indeed, previous studies have found that CCR5 acts in tumor cells to promote stem cell expansion and metastasis in breast cancer (Jiao et al., 2018; Velasco-Velazquez et al., 2012). Although in the current study we find that in residual tumors CCR5 is expressed at higher levels in macrophages than on tumor cells, it is possible that tumor cell-expressed CCR5 may mediate at least some of the effects of

CCL5 on tumor recurrence. Future work with mice lacking CCR5 on specific cell types will clarify the relative importance of CCR5 on macrophages and tumor cells.

The survival and recurrence of residual tumor cells is a critical clinical problem in breast cancer. The results identified here show that interactions between residual tumor cells and their microenvironment are critical for recurrent tumor formation. Targeting tumor cell-microenvironment interactions may hold promise for preventing recurrent breast cancer.

MATERIALS AND METHODS

Key resources table

Reagent type (species) or resource	Designation	Source or reference	Identifiers	Additional Information
Recombinant DNA reagent	pLenti CMV GFP Neo	Addgene	Plasmid # 17447 RRID:Addgene_17447	Campeau et al PLoS One. 2009 Aug 6;4(8):e6529
Recombinant DNA reagent	lentiCas9-Blast	Addgene	Plasmid # 52962 RRID:Addgene_52962	Sanjana et al Nat Methods. 2014 Aug;11(8):783-4
Recombinant DNA reagent	lentiGuide-Puro	Addgene	Plasmid # 52963 RRID:Addgene_52963	Sanjana et al Nat Methods. 2014 Aug;11(8):783-4
Recombinant DNA reagent	psPAX2	Addgene	Plasmid # 12260 RRID:Addgene_12260	Trono Lab Packing and Envelope Plasmids
Recombinant DNA reagent	pMD2.G	Addgene	Plasmid# 12259 RRID:Addgene_12259	Trono Lab Packing and Envelope Plasmids

Cell line (<i>M. musculus</i>)	NIH-3T3	American Type Culture Collection	Cat# CRL-1658 RRID:CVCL_0594	
Cell line (<i>M. musculus</i>)	54074	This paper		Derived from MTB;TAN model
Cell line (<i>M. musculus</i>)	99142	This paper		Derived from MTB;TAN model
Cell line (<i>H. Sapiens</i>)	293T Ampho	American Type Culture Collection	Cat# CRL-3213 RRID:CVCL_H716	
Cell line (<i>H. Sapiens</i>)	293T Eco	American Type Culture Collection	Cat# CRL-3214 RRID:CVCL_H717	
Antibody	Rabbit monoclonal anti-NFκB p65	Cell Signaling	D14E12 RRID:AB_10859369	1:1000 (WB)
Antibody	Rabbit monoclonal anti-p-NFκB p65	Cell Signaling	93H1 RRID:AB_10827881	1:1000 (WB)
Antibody	Mouse monoclonal anti-Tubulin	Santa Cruz	TU-02 RRID:AB_628408	1:1000 (WB)
Antibody	Goat anti-rabbit HRP	Cell Signaling	Cat# 7074 RRID:AB_2099233	1:5000 (WB)
Antibody	Goat anti-mouse HRP	Cell Signaling	Cat# 7076 RRID:AB_330924	1:5000 (WB)
Antibody	Goat anti-rabbit Alexa Flour 680	Life Technologies	Cat# A21076 RRID:AB_141386	1:5000 (WB)

Antibody	IRDYE 800CW Goat anti-mouse	LI-COR	Cat# 926- 32210 RRID:AB_6 21842	1:5000 (WB)
Antibody	Rat monoclonal anti- CD45R/B22 0, APC conjugated	Invitrogen/eBios cience (Carlsbad, CA)	RA3-6B2 RRID:AB_4 69395	1:50 (FC)
Antibody	Hamster monoclonal anti-CD49b, AF488 conjugated	BioLegend	HMα2 RRID:AB_4 92851	1:200 (FC)
Antibody	Hamster monoclonal anti-FcεRIα, PE conjugated	BioLegend	1-Mar RRID:AB_1 626104	1:50 (FC)
Antibody	Rat monoclonal anti-Siglec- F/CD170, PE conjugated	BD	E50-2440 RRID:AB_1 0896143	1:200 (FC)
Antibody	Rat monoclonal anti- PDGFRα/CD 140a, PE conjugated	Invitrogen/eBios cience	APA5 RRID:AB_6 57615	1:100 (FC)
Antibody	Rat monoclonal anti-CD45, PECy5 conjugated	BD	30-F11 RRID:AB_3 94612	1:200 (FC)
Antibody	Mouse monoclonal anti-CD45, APC conjugated	BD	30-F11 RRID:AB_1 645215	1:200 (FC)
Antibody	Rat anti- CD45, V50 conjugated	BD	30-F11 RRID:AB_1 645275	1:200 (FC)

Antibody	Rat monoclonal anti-F4/80, AF647 conjugated	BD	T45-2342 RRID:AB_2744474	1:50 (FC)
Antibody	Rat monoclonal anti-CD11b, PE conjugated	BD	M1/70 RRID:AB_394775	1:50 (FC)
Antibody	Rat monoclonal anti-CD11b, PECy7 conjugated	BD	M1/70 RRID:AB_2033994	1:100 (FC)
Antibody	Rat monoclonal anti-Ly6G, APC conjugated	BD	1A8 RRID:AB_1727560	1:200 (FC)
Antibody	Hamster monoclonal anti-CD3e, PE conjugated	BD	145-2C11 RRID:AB_394460	1:100 (FC)
Antibody	Rat monoclonal anti-CD4, APCC7y conjugated	BD	GK1.5 RRID:AB_394331	1:100 (FC)
Antibody	Rat monoclonal anti-CD8a, APC conjugated	BD	53-6.7 RRID:AB_398527	1:200 (FC)
Antibody	Rat monoclonal anti-CD16/CD32 Fc Blocker	BD	2.4G2 RRID:AB_394659	1:50 (FC)
Antibody	Rat monoclonal anti-CCR5/CD19 5, BV421 conjugated	BD	C34-3448 RRID:AB_2741677	1:100 (FC)

Antibody	Mouse monoclonal anti-Cytokertin 8	Troma 1, Brulet, P., Kemler, R. Institut Pasteur, Paris, France	Troma 1 RRID:AB_531826	1:50 (IHC)
Antibody	Rat monoclonal anti-CD45	BD Biosciences	30-F11 RRID:AB_394606	1:200 (IHC)
Antibody	Rabbit monoclonal anti-CD3	Thermo	SP7 RRID:AB_1956722	1:100 (IHC)
Antibody	Rat monoclonal anti-F4/80	Bio-Rad	Cl:A3-1 RRID:AB_1102558	1:1000 (IHC)
Peptide, recombinant protein	TNF α , mouse	BioLegend	Cat# 575202	10 ng/mL
Commercial assay or kit	Trichrome stain	Abcam	ab150686	
Commercial assay or kit	Vectastain ABC Kit (Rabbit IgG)	Vector Labs	Cat# PK-6101	
Commercial assay or kit	Vectastain ABC Kit (Rat IgG)	Vector Labs	Cat# PK-4004	
Commercial assay or kit	RNeasy Mini Kit	Qiagen	Qiagen:74106	
Commercial assay or kit	QIAshredder	Qiagen	Qiagen:79656	
Commercial assay or kit	Quantibody Mouse Cytokine Array Q1	RayBiotech	Cat# QAM-CYT-1-1	
Commercial	Quantibody Mouse	RayBiotech	Cat# QAM-CYT-4	

assay or kit	Cytokine Array Q4			
Chemical compound, drug	IKK16	Selleckchem	Cat# S2882	100nM
Chemical compound, drug	Lipofectamine 2000	Life Technologies	Cat# 11668019	60 μ L per reaction
Chemical compound, drug	Polybrene	Sigma	Cat# 107689	6 μ g/mL
Chemical compound, drug	2x Cell Lysis Buffer	RayBiotech	Cat# AA-LYS	
Chemical compound, drug	Luminata Classico/Crescendo Western HRP Substrate	Millipore	Cat#WBLU C0500 Cat# WBLUR0500	
Chemical compound, drug	Doxycycline	RPI	Cat# D43020-100.0	2 mg/kg <i>in vivo</i> and 2 μ g/mL <i>in vitro</i>
Sequence-based reagent	RT-PCR primers	This paper	CCL5 cDNA into pK1 plasmid	Forward: TAACCTCGAGATGAAGATC TCTGCAGCTG, Reverse: TAACGCGGCCGCCAGGGTC AGAATCAAGAAACC
Sequence-based reagent	RT-PCR primers	This paper	CCL5 cDNA into pLenti CMV plasmid	Forward: TAACTCTAGAATGAAGATC TCTGCAGCTG, Reverse: TAACGTCGACCAGGGTCAG AATCAAGAAACC

Sequen ce- based reagent	gRNAs	This paper	Targeting CCL5	CCL5_1 (TG TAGAAATACTCCTTGAC G), CCL5_2 (TACTCCTTGACGTGGGCAC G), CCL5_3 (TGCAGAGGGCGGCTGCAGT G)
Sequen ce- based reagent	CCL5	Thermo	Mm0130242 7_m1	
Sequen ce- based reagent	CXCL1	Thermo	Mm0420746 0_m1	
Sequen ce- based reagent	CXCL2	Thermo	Mm0043645 0_m1	
Sequen ce- based reagent	CXCL5	Thermo	Mm0043645 1_g1	
Sequen ce- based reagent	CCL2	Thermo	Mm0044124 2_m1	
Sequen ce- based reagent	Actin	Thermo	Mm0261958 0_g1	
Sequen ce- based reagent	ASPN	Thermo	Mm0044594 5_m1	
Sequen ce- based reagent	PCOLCE	Thermo	Mm0047660 8_m1	
Sequen ce- based reagent	COL5A1	Thermo	Mm0048929 9_m1	
Sequen ce-	COL24A1	Thermo	Mm0132374 4_m1	

based reagent				
Software, algorithm	GraphPad Prism	GraphPad Prism (https://graphpad.com)	RRID:SCR_002798	Version 8
Software, algorithm	JMP Pro	SAS Institute Inc., Cary, NC		
Software, algorithm	FlowJo	TreeStar	RRID:SCR_008520	
Software, algorithm	Fiji	Fiji (http://fiji.nih.gov/)	RRID:SCR_002285	Schindelin, J.; Arganda-Carreras, I. & Frise, E. et al. (2012) Nature methods 9(7):676-682

WB = Western blot, FC = flow cytometry, IHC = immunohistochemistry

Orthotopic recurrence assays

Orthotopic tumor recurrence assays were performed as described (Alvarez et al. 2013). Briefly, cohorts of 6-week old recipient mice (nu/nu or TAN) on doxycycline were injected bilaterally in the #4 inguinal mammary fat pad with 1×10^6 primary tumor cells (expressing either a control sgRNA, a sgRNA targeting CCL5, CCL5 cDNA, or GFP cDNA). Once tumors reached 5 mm (2-3 weeks), doxycycline was removed to initiate oncogene down-regulation and tumor regression. Mice were palpated biweekly to monitor tumor recurrence, and sacrificed when recurrent tumors reached 10 mm. Differences in recurrence-free survival between control and experimental cohorts were compared using Kaplan-Meier survival curves (L et al., 1958) and evaluated by the p-value from a log-rank test and the hazard ratio from the Cox proportional hazard regression, as described previously (Alvarez et al., 2013).

Power calculations were used to determine cohort size for each in vivo experiment. Briefly, in order to detect a 2.5-fold difference in recurrence-free survival between control and

experimental groups, given a median recurrence-free survival of 60 days for the control group and a 300-day follow-up, we estimated we would need to enroll 22 tumors per group (80% power, $p < 0.05$). We enrolled extra mice in each cohort to account for tumor take rates and unexpected mortality. Final cohort sizes were: GFP tumors, 17 mice (34 tumors); CCL5 tumors, 18 mice (36 tumors); sgControl tumors, 20 mice (40 tumors); sgCCL5 tumors, 20 mice (40 tumors).

Tissue culture and reagents

Cell lines derived from primary MTB;TAN tumors were grown as previously described in media containing 2 $\mu\text{g/ml}$ dox (Alvarez et al., 2013). For conditioned media experiments, primary tumor cell lines were plated on 10-cm plates. 24 hours later, media was changed to media without dox, and conditioned media was collected one or two days later. Media was centrifuged to remove cells, supplemented with 2 $\mu\text{g/ml}$ dox, and applied to naïve primary tumor cells. Cells treated with conditioned media were harvested one or two days later for qPCR or Western blot analysis. For dox withdrawal experiments, primary tumor cell lines were plated 10-cm plates. 24 hours later, media was changed to media without dox and cells were collected one or two days later for qPCR or Western blot analysis. IKK16 (Selleckchem, Houston, TX) was used at 100 nM, TNF α (BioLegend, San Diego, CA) was used at 10 ng/ml.

Primary cells derived from MTB;TAN tumors (54074 and 99142 cells) were generated by our lab, are used at early passages, and as a result have not been authenticated. NIH3T3 cells were tested by the Duke Cell Culture Facility for mycoplasma contamination and tested negative. The facility was not able to perform STR authentication on these mouse cells.

Flow cytometry

Tumors were harvested and digested as previously described (Mabe et al., 2018). Cells were aliquoted at 1×10^6 cells per 5 mL falcon tube. CD16/CD32 Fc Block antibody was added for 10 min at 4°C (2 μ L/ 1×10^6 cells). Tumors were then stained with antibody cocktails listed below for 30 min at 4°C, and then washed 3 times with FACs buffer (BD Biosciences, Billerica, MA).

Cell Type	Antibody	Fluorophore	Clone	Vendor	Dilution
B Cell	CD45R/B220	APC	RA3-6B2	Invitrogen/eBioscience (Carlsbad, CA)	1:50
Basophil	CD49b	AF488	HM α 2	BioLegend	1:200
Basophil	Fc ϵ RI α	PE	MAR-1	BioLegend	1:50
Eosinophil	Siglec-F/CD170	PE	E50-2440	BD	1:200
Fibroblast	PDGFR α /CD140a	PE	APA5	Invitrogen/eBioscience	1:100
Leukocyte	CD45	PECy5	30-F11	BD	1:200
Leukocyte	CD45	APC	30-F11	BD	1:200
Leukocyte	CD45	V450	30-F11	BD	1:200
Macrophage	F4/80	AF647	T45-2342	BD	1:50
Monocyte/Granulocyte	CD11b	PE	M1/70	BD	1:50
Monocyte/Granulocyte	CD11b	PECy7	M1/70	BD	1:100
Neutrophil	Ly6G	APC	1A8	BD	1:200
T Cell	CD3e	PE	145-2C11	BD	1:100
T Cell	CD4	APCCy7	GK1.5	BD	1:100
T Cell	CD8a	APC	53-6.7	BD	1:200
-	Fc Blocker	-	2.4G2	BD	1:50
-	CCR5/CD195	BV421	C34-3448	BD	1:100

Cells were analyzed using a FACSCanto analyzer (BD Biosciences) and data were analyzed using FlowJo software (TreeStar, Ashland, OR). Gating of the CCR5-high population was determined by using a fluorescence minus one (FMO; cells stained with antibodies for cell type markers, lacking the CCR5 antibody) histogram in the fluorescence channel for the CCR5 antibody as a

negative control. The FMO negative control histogram was plotted with a positive control of the single stain (cells stained only with CCR5 antibody) from the same tumor. Percent of CCR5+ cells were gated according to the positive control.

qPCR

RNA was isolated from tumors and cells using RNeasy columns (Qiagen, Hilden, Germany). 1 µg of RNA was reversed transcribed using cDNA synthesis reagents (Promega, Madison, WI). qPCR was performed using 6-carboxyfluorescein labeled TaqMan probes (Thermo, Waltham, MA): CCL5 (Mm01302427_m1), CXCL1 (Mm04207460_m1), CXCL2 (Mm00436450_m1), CXCL5 (Mm00436451_g1), CCL2 (Mm00441242_m1), Actin (Mm02619580_g1), ASPN (Mm00445945_m1), PCOLCE (Mm00476608_m1), COL5A1 (Mm00489299_m1), COL24A1 (Mm01323744_m1), and read on a Bio-Rad (Hercules, CA) CFX qPCR machine.

Western blotting and cytokine arrays

Western blotting was performed as described (Alvarez et al. 2013) using the following antibodies: NFκB p65 (D14E12, Cell Signaling, Danvers, MA), p-NFκB p65 (93H1, Cell Signaling), and tubulin (TU-02, Santa Cruz, Dallas, TX), all at a 1:1000 dilution. Secondary antibodies conjugated to Alexa Flour 680 (Life Technologies, Carlsbad, CA) or 800 (LI-COR Biosciences, Lincoln, NE) were detected with the Odyssey detection system (LI-COR Biosciences). For p-p65 detection, secondary antibodies conjugated to HRP were used and blots were developed using Classico or Crescendo reagent (Millipore, Burlington, MA) and exposed to film (VWR, Radnor, PA). Secondary antibodies were used at a 1:5000 dilution.

For cytokine array analysis, tumor lysates were made in 2X lysis buffer (RayBiotech, Norcross, GA) and diluted to 50 µg per 100 µL in diluent provided. Tumor lysates and standards

were run on both Quantibody Mouse Cytokine Array Q1 and Q4 (RayBiotech). Slides were scanned and quantified by RayBiotech.

Plasmids and CRISPR/Cas9

pLenti CMV GFP Puro was purchased from Addgene (Watertown, MA).

A CCL5 cDNA encoding the full-length mouse protein was amplified by RT-PCR from recurrent MTB;TAN tumor cells and cloned into the retroviral expression vector pK1 using the following primers: Forward: TAACCTCGAGATGAAGATCTCTGCAGCTG, Reverse: TAACGCGGCCGCCAGGGTCAGAATCAAGAAACC.

A CCL5 cDNA encoding the full-length mouse protein was amplified by RT-PCR from recurrent MTB;TAN tumor cells and cloned into the lentiviral expression vector pLenti CMV using the following primers: Forward: TAACTCTAGAATGAAGATCTCTGCAGCTG, Reverse: TAACGTCGACCAGGGTCAGAATCAAGAAACC.

CCL5 CRISPR sgRNAs: CCL5_1 (TG TAGAAATACTCCTTGACG), CCL5_2 (TACTCCTTGACGTGGGCACG), CCL5_3 (TGCAGAGGGCGGCTGCAGTG). A small guide against AAVS was used as control. sgRNAs were cloned into Lentiguide puro (Sanjana et al. 2014). Cas9 infection was with lentiguide Cas9 blast (Sanjana et al. 2014).

Retrovirus was produced by transfecting the packaging lines 293T Amphi and 293T Eco with the retroviral construct pK1 empty or CCL5 using Lipofectamine 2000. Retroviral supernatant was collected 48 hours post-transfection, filtered, and used to transduce cells in the presence of 6 µg/mL polybrene (Sigma, St. Louis, MO).

Lentivirus was produced by transfecting 293T cells with the packaging plasmids psPAX2 and pMD2.G and lentiviral construct pLenti CMV GFP or CCL5 using Lipofectamine 2000.

Lentiviral supernatant was collected 48 hours post-transfection, filtered, and used to transduce cells in the presence of 6 µg/mL polybrene (Sigma).

RNA sequencing

RNA was isolated from tumors or tumor cells using RNeasy columns (Qiagen). For TAM sequencing, macrophages were isolated by FACS using the antibody panel described above, and RNA was isolated using RNeasy columns (Qiagen). RNA was sequenced using the Illumina HiSeq 4000 libraries and sequencing platform with 50 base pair single end reads by the Duke GCB Sequencing and Genomic Technologies Shared Resource (Durham, NC). Sequencing data have been deposited in SRA as PRJNA506006 for cell line data and PRJNA505845 for macrophage data.

Human breast cancer microarray data

Publicly available microarray data from human primary and residual breast cancer datasets GSE10281 and GSE21974 and their corresponding clinical annotation were downloaded, converted to log2 scale, and median centered. Heatmaps were created using R (Team, 2013).

Immunohistochemistry and staining

Tumor sections were fixed in 10% normal formalin for 16 hours, then washed twice with PBS and transferred to 70% ethanol for storage. Stored tumor sections were paraffin imbedded and cut on the microtome in 5 µm sections. Sections were stained using a regressive H&E protocol, immunohistochemistry, or Masson's Trichrome.

The regressive H&E protocol is as follows: dewax and rehydrate slides. Incubate slides in Harris Modified Hematoxylin with Acetic Acid (Fisher, Hampton, NH) for 5 min. Incubate in Eosin (Sigma) for 1:30 min. Then dehydrate slides and mount slides with permount and coverslip. Let dry overnight.

For cytokeratin 8 staining (Troma 1, Brulet, P., Kemler, R. Institut Pasteur, Paris, France) immunohistochemistry slides were dewaxed and rehydrated as above. Slides were boiled in antigen retrieval buffer (1X in ddH₂O) for 5 minutes and allowed to cool. Slides were washed in PBS and then incubated in 0.3% H₂O₂. Slides were washed, blocked and stained according to the protocol from the rabbit secondary Vectastain ABC kit (Vector Labs, Burlingame, CA). Primary antibody was used at a dilution of 1:50. CD45 (30-F11, BD Biosciences, 1:200), CD3 (SP7, Thermo, 1:100), and F4/80 (Cl:A3-1, Bio-Rad, 1:1000) staining were performed by the Duke Pathology core (Durham, NC).

Trichrome stain was performed using a staining kit from Abcam (Cambridge, UK) (ab150686).

Quantifying IHC and Masson's Trichrome in Fiji

To quantify the amount of positive staining for CD3, CD45, and F4/80 and for Masson's Trichrome, we used Fiji (Schindelin et al., 2012). The 'Color Deconvolution' function was used to separate the colors into positive staining and hematoxylin for normalization. We then converted each image to 8-bit and applied a threshold of positive staining to each image and used this same threshold across all images. We then measured the pixel area of the positive staining and normalized this to the hematoxylin staining for each image. For the primary tumors and 5-day -dox tumors, the whole image was used for quantification. For residual tumors we manually selected regions-of-interest to exclude adipose tissue from the quantification.

Statistical reporting

For GSEA, the normalized enrichment score (NES) is reported. The normalized enrichment score accounts for differences in gene set size and in correlations between gene sets. The NES is based on all dataset permutations, to correct for multiple hypothesis testing. The nominal p value

is also reported, and is the statistical significance of the enrichment score, without adjustment for gene set size or multiple hypothesis testing. A reported p value of zero (0.0) indicates an actual p-value of less than 1/number-of-permutations. (Subramanian et al., 2005)

Two-tailed unpaired t-tests were used to analyze significance between primary tumor samples and all other time points for qPCR, cytokine array, and flow cytometry analysis. For the cytokine array, appropriate sample size was calculated using JMP Pro (SAS Institute Inc., Cary, NC). A standard deviation of 20% was assumed, with a power of 0.8, fold change of 2, and p-value (alpha) of 0.05. This power calculation indicated that a sample size of 8 (4 tumors per cohort) was required. The same parameters were used for sample size calculation for flow cytometry analysis of control and CCL5-expressing tumors. For recurrence free survival (RFS), statistical analysis methods are listed in orthotopic recurrence assays.

Outliers were never excluded except for in flow cytometry experiments. Tumors that were >90% CD45+ were excluded from analysis to avoid analyzing tumors with potential contamination from the inguinal lymph node. For all other experiments where no power analysis was used, sample size was chosen based upon previous experience (Alvarez et al., 2013).

Study approval

Animal care and all animal experiments were performed with the approval of and in accordance with Duke University IACUC guidelines. Mice were housed under barrier conditions.

Funding

This work was funded by the National Cancer Institute (R01 CA208042 to JVA and F31 CA220957 to AW) and by startup funds from the Duke Cancer Institute, the Duke University School of Medicine and the Whitehead Foundation (to JVA).

Acknowledgements

We thank Cui Rong (Duke-NUS, Singapore) for providing technical assistance, as well as members of the Alvarez lab for providing assistance and helpful discussions. We thank Dr. Mike Cook (Duke University) and Dr. Brent Hanks (Duke University) for assistance with flow cytometry. We thank Dr. So Young Kim (Duke University) for reagents for the CRISPR-Cas9 cell lines. We also thank Dr. Donald McDonnell, Dr. Binita Das, and Dr. Ching-Yi Chang (Duke University) for providing assistance and reagents for flow cytometry.

REFERENCES

- Afik, R., Zigmond, E., Vugman, M., Klepfish, M., Shimshoni, E., Pasmanik-Chor, M., Shenoy, A., Bassat, E., Halpern, Z., Geiger, T., *et al.* (2016). Tumor macrophages are pivotal constructors of tumor collagenous matrix. *The Journal of experimental medicine* *213*, 2315-2331.
- Aldinucci, D., and Colombatti, A. (2014). The inflammatory chemokine CCL5 and cancer progression. *Mediators of inflammation* *2014*, 292376.
- Alexander-Savino, C.V., Hayden, M.S., Richardson, C., Zhao, J., and Poligone, B. (2016). Doxycycline is an NF- κ B inhibitor that induces apoptotic cell death in malignant T-cells. *Oncotarget* *7*, 75954-75967.
- Alvarez, J.V., Pan, T.-c., Ruth, J., Feng, Y., Zhou, A., Pant, D., Grimley, J.S., Wandless, T.J., DeMichele, A., and Chodosh, L.A. (2013). Par-4 Downregulation Promotes Breast Cancer Recurrence by Preventing Multinucleation following Targeted Therapy. *Cancer cell* *24*, 30-44.
- Araujo, J.M., Gomez, A.C., Aguilar, A., Salgado, R., Balko, J.M., Bravo, L., Doimi, F., Bretel, D., Morante, Z., Flores, C., *et al.* (2018). Effect of CCL5 expression in the recruitment of immune cells in triple negative breast cancer. In *Scientific reports*, pp. 4899.
- Binnewies, M., Roberts, E.W., Kersten, K., Chan, V., Fearon, D.F., Merad, M., Coussens, L.M., Gabrilovich, D.I., Ostrand-Rosenberg, S., Hedrick, C.C., *et al.* (2018). Understanding the tumor immune microenvironment (TIME) for effective therapy. *Nature medicine*, 1-10.
- Creighton, C.J., Li, X., Landis, M., Dixon, J.M., Neumeister, V.M., Sjolund, A., Rimm, D.L., Wong, H., Rodriguez, A., Herschkowitz, J.I., *et al.* (2009). Residual breast cancers after conventional therapy display mesenchymal as well as tumor-initiating features. *Proceedings of the National Academy of Sciences of the United States of America* *106*, 13820-13825.
- Damrauer, J.S., Phelps, S.N., Amuchastegui, K., Lupo, R., Mabe, N.W., Walens, A., Kroger, B.R., and Alvarez, J.V. (2018). Foxo-dependent Par-4 Upregulation Prevents Long-term Survival of Residual Cells Following PI3K–Akt Inhibition. *Molecular Cancer Research*.
- Dembic, Z. (2015). *Cytokines of the Immune System: Chemokines* (Academic Press).
- DeNardo, D.G., Brennan, D.J., Rexhepaj, E., Ruffell, B., Shiao, S.L., Madden, S.F., Gallagher, W.M., Wadhwani, N., Keil, S.D., Junaid, S.A., *et al.* (2011). Leukocyte Complexity Predicts Breast Cancer Survival and Functionally Regulates Response to Chemotherapy. *Cancer discovery* *1*, 54-67.
- Flores-Borja, F., Irshad, S., Gordon, P., Wong, F., Sheriff, I., Tutt, A., and Ng, T. (2016). Crosstalk between Innate Lymphoid Cells and Other Immune Cells in the Tumor Microenvironment. *Journal of Immunology Research* *2016*, 1-14.
- Gong, K., Guo, G., Gerber, D.E., Gao, B., Peyton, M., Huang, C., Minna, J.D., Hatanpaa, K.J., Kernstine, K., Cai, L., *et al.* (2018). TNF-driven adaptive response mediates resistance to EGFR inhibition in lung cancer. *The Journal of clinical investigation* *128*, 2500-2518.

563 Hata, A.N., Niederst, M.J., Archibald, H.L., Gomez-Caraballo, M., Siddiqui, F.M., Mulvey,
564 H.E., Maruvka, Y.E., Ji, F., Bhang, H.-e.C., Krishnamurthy Radhakrishna, V., *et al.* (2016).
565 Tumor cells can follow distinct evolutionary paths to become resistant to epidermal growth
566 factor receptor inhibition. *Nature medicine* 22, 262-269.

567 Holohan, C., Van Schaeybroeck, S., Longley, D.B., and Johnston, P.G. (2013). Cancer drug
568 resistance: an evolving paradigm. *Nature Reviews Cancer* 13, 714.

569 Hölzel, D., Eckel, R., Emeny, R.T., and Engel, J. (2010). Distant metastases do not metastasize.
570 *Cancer and Metastasis Reviews* 29, 737-750.

571 Hudson, A.L., Parker, N.R., Khong, P., Parkinson, J.F., Dwight, T., Ikin, R.J., Zhu, Y., Chen, J.,
572 Wheeler, H.R., and Howell, V.M. (2018). Glioblastoma Recurrence Correlates With Increased
573 APE1 and Polarization Toward an Immuno-Suppressive Microenvironment. *Frontiers in*
574 *oncology* 8, 314-314.

575 Jiao, X., Velasco-Velazquez, M.A., Wang, M., Li, Z., Rui, H., Peck, A.R., Korkola, J.E., Chen,
576 X., Xu, S., DuHadaway, J.B., *et al.* (2018). CCR5 Governs DNA Damage Repair and Breast
577 Cancer Stem Cell Expansion. *Cancer research* 78, 1657-1671.

578 Klein, C.A. (2009). Parallel progression of primary tumours and metastases. *Nature Reviews*
579 *Cancer* 9, 302.

580 L, E., Kaplan, and Meier, P. (1958). Nonparametric Estimation From Incomplete Observations.
581 *Journal of the American Statistical Association* 53, 457-481.

582 Lacy, P. (2017). Eosinophil Cytokines in Allergy. In (Academic Press), pp. 173-218.

583 Lee, C.-M., Peng, H.-H., Yang, P., Liou, J.-T., Liao, C.-C., and Day, Y.-J. (2017). C-C
584 Chemokine Ligand-5 is critical for facilitating macrophage infiltration in the early phase of liver
585 ischemia/reperfusion injury. *Scientific Reports* 7, 3698.

586 Lee, R.J., Albanese, C., Fu, M., Amico, M., Lin, B., Watanabe, G., Haines, G.K., Siegel, P.M.,
587 Hung, M.-C., Yarden, Y., *et al.* (2000). Cyclin D1 Is Required for Transformation by Activated
588 Neu and Is Induced through an E2F-Dependent Signaling Pathway. *Molecular and cellular*
589 *biology* 20, 672.

590 Liu, M., Ju, X., Willmarth, N.E., Casimiro, M.C., Ojeifo, J., Sakamaki, T., Katiyar, S., Jiao, X.,
591 Popov, V.M., Yu, Z., *et al.* (2009). Nuclear factor-kappaB enhances ErbB2-induced mammary
592 tumorigenesis and neoangiogenesis in vivo. *The American journal of pathology* 174, 1910-1920.

593 Liu, M., Sakamaki, T., Casimiro, M.C., Willmarth, N.E., Quong, A.A., Ju, X., Ojeifo, J., Jiao,
594 X., Yeow, W.-S., Katiyar, S., *et al.* (2010). The canonical NF-kappaB pathway governs
595 mammary tumorigenesis in transgenic mice and tumor stem cell expansion. *Cancer research* 70,
596 10464-10473.

597 López, Á.G., Seoane, J.M., and Sanjuán, M.A.F. (2017). Dynamics of the cell-mediated immune
598 response to tumour growth. *Phil Trans R Soc A* 375, 20160291-20160214.

599 Lu, P., Weaver, V.M., and Werb, Z. (2012). The extracellular matrix: A dynamic niche in cancer
600 progression. *J Cell Biol* 196, 395-406.

601 Lu, X., Mu, E., Wei, Y., Riethdorf, S., Yang, Q., Yuan, M., Yan, J., Hua, Y., Tiede, B.J., Lu, X.,
602 *et al.* (2011). VCAM-1 Promotes Osteolytic Expansion of Indolent Bone Micrometastasis of
603 Breast Cancer by Engaging $\alpha 4 \beta 1$ -Positive Osteoclast Progenitors. *Cancer cell* 20, 701-714.

604 Mabe, N.W., Fox, D.B., Lupo, R., Decker, A.E., Phelps, S.N., Thompson, J.W., and Alvarez,
605 J.V. (2018). Epigenetic silencing of tumor suppressor Par-4 promotes chemoresistance in
606 recurrent breast cancer. *The Journal of clinical investigation* 128, 4413-4428.

607 Meads, M.B., Gatenby, R.A., and Dalton, W.S. (2009). Environment-mediated drug resistance: a
608 major contributor to minimal residual disease. *Nature Reviews Cancer* 9, 665.

609 Moody, S.E. (2002). Conditional activation of Neu in the mammary epithelium of transgenic
610 mice results in reversible pulmonary metastasis. *Cancer cell* 2, 451-461.

611 Neville-Webbe, H.L., Cross, N.A., Eaton, C.L., Nyambo, R., Evans, C.A., Coleman, R.E., and
612 Holen, I. (2004). Osteoprotegerin (OPG) produced by bone marrow stromal cells protects breast
613 cancer cells from TRAIL-induced apoptosis. *Breast cancer research and treatment* 86, 269-279.

614 Pollard, J.W. (2004). Opinion: Tumour-educated macrophages promote tumour progression and
615 metastasis. *Nature Reviews Cancer* 4, 71-78.

616 Provenzano, P.P., Inman, D.R., Eliceiri, K.W., Knittel, J.G., Yan, L., Rueden, C.T., White, J.G.,
617 and Keely, P.J. (2008). Collagen density promotes mammary tumor initiation and progression.
618 *BMC Medicine* 6, 11.

619 Santa-Cecília, F.V., Socias, B., Ouidja, M.O., Sepulveda-Diaz, J.E., Acuña, L., Silva, R.L.,
620 Michel, P.P., Del-Bel, E., Cunha, T.M., and Raisman-Vozari, R. (2016). Doxycycline Suppresses
621 Microglial Activation by Inhibiting the p38 MAPK and NF- κ B Signaling Pathways.
622 *Neurotoxicity Research* 29, 447-459.

623 Schindelin, J., Arganda-Carreras, I., Frise, E., Kaynig, V., Longair, M., Pietzsch, T., Preibisch,
624 S., Rueden, C., Saalfeld, S., Schmid, B., *et al.* (2012). Fiji: an open-source platform for
625 biological-image analysis. *Nature methods* 9, 676-682.

626 Sequist, L.V., Waltman, B.A., Dias-Santagata, D., Digumarthy, S., Turke, A.B., Fidias, P.,
627 Bergethon, K., Shaw, A.T., Gettinger, S., Cosper, A.K., *et al.* (2011). Genotypic and histological
628 evolution of lung cancers acquiring resistance to EGFR inhibitors. *Science translational medicine*
629 3, 75ra26-75ra26.

630 Sharma, S.V., Lee, D.Y., Li, B., Quinlan, M.P., Takahashi, F., Maheswaran, S., McDermott, U.,
631 Azizian, N., Zou, L., Fischbach, M.A., *et al.* (2010). A Chromatin-Mediated Reversible Drug-
632 Tolerant State in Cancer Cell Subpopulations. *Cell* 141, 69-80.

633 Soria, G., and Ben-Baruch, A. (2008). The inflammatory chemokines CCL2 and CCL5 in breast
634 cancer. *Cancer letters* 267, 271-285.

635 Sosa, M.S., Avivar-Valderas, A., Bragado, P., Wen, H.-C., and Aguirre-Ghiso, J.A. (2011).
636 ERK1/2 and p38 α / β Signaling in Tumor Cell Quiescence: Opportunities to Control Dormant
637 Residual Disease. *Clinical Cancer Research* 17, 5850-5857.

638 Strachan, D.C., Ruffell, B., Oei, Y., Bissell, M.J., Coussens, L.M., Pryer, N., and Daniel, D.
639 (2014). CSF1R inhibition delays cervical and mammary tumor growth in murine models by
640 attenuating the turnover of tumor-associated macrophages and enhancing infiltration by CD8 +T
641 cells. *Oncoimmunology* 2, e26968-26913.

642 Subramanian, A., Tamayo, P., Mootha, V.K., Mukherjee, S., Ebert, B.L., Gillette, M.A.,
643 Paulovich, A., Pomeroy, S.L., Golub, T.R., Lander, E.S., *et al.* (2005). Gene set enrichment
644 analysis: a knowledge-based approach for interpreting genome-wide expression profiles.
645 *Proceedings of the National Academy of Sciences of the United States of America* 102, 15545-
646 15550.

647 Team, R.C. (2013). R: A language and environment for statistical computing. . R Foundation for
648 Statistical Computing, Vienna, Austria.

649 Tempfer, C. (2011). Basal-like molecular subtype and HER4 up-regulation and response to
650 neoadjuvant chemotherapy in breast cancer. *Oncology reports*.

651 Thannickal, V.J. (2012). Mechanisms of pulmonary fibrosis: role of activated myofibroblasts and
652 NADPH oxidase. *Fibrogenesis & tissue repair* 5, S23-S23.

653 Velasco-Velazquez, M., Jiao, X., De La Fuente, M., Pestell, T.G., Ertel, A., Lisanti, M.P., and
654 Pestell, R.G. (2012). CCR5 Antagonist Blocks Metastasis of Basal Breast Cancer Cells. *Cancer*
655 *research* 72, 3839-3850.

656 Zhu, Y., Knolhoff, B.L., Meyer, M.A., Nywening, T.M., West, B.L., Luo, J., Wang-Gillam, A.,
657 Goedegebuure, S.P., Linehan, D.C., and DeNardo, D.G. (2014). CSF1/CSF1R Blockade
658 Reprograms Tumor-Infiltrating Macrophages and Improves Response to T-cell Checkpoint
659 Immunotherapy in Pancreatic Cancer Models. *Cancer research* 74, 5057-5069.
660
661

Figure Legends

Figure 1) Her2 downregulation induces an inflammatory gene expression program driven by the TNF α /IKK pathway. (a) RNA-seq analysis of two independent primary Her2-driven tumor cell lines in the presence of Her2 expression (+dox) or two days following Her2 downregulation (-dox). The heatmap shows the top 100 differentially expressed genes between +dox and -dox conditions. R1 and R2 are biological replicates. **(b)** Gene set enrichment analysis (GSEA) of RNA-seq data showing enrichment of an inflammatory response signature and a TNF α /NF- κ B signature in cells following Her2 downregulation. P-values and normalized enrichment scores (NES) are shown. **(c)** Heatmap showing expression of select genes from the TNF α /NF- κ B signature in the presence of Her2 expression (+dox) or following Her2 deinduction (-dox). **(d)** qRT-PCR analysis of CCL5 expression following 1 or 2-day treatment with conditioned media harvested from primary cells following Her2 downregulation. Dox was added to conditioned media prior to treatment to maintain Her2 expression in target cells. Results shown are representative of two independent experiments. **(e)** qRT-PCR of TNF α expression in primary cells in the presence of Her2 expression (+dox) or 2 and 4 days following Her2 downregulation. Results shown are representative of two independent experiments. **(f)** Primary tumor cells were treated with conditioned media as described in (d), and activation of the NF- κ B pathway was assessed by Western blot analysis of total and phospho-p65. Results show 3 biological replicates per time point. **(g)** qRT-PCR analysis of the indicated genes in primary tumor cells in the presence of Her2 expression (+dox) or 1 and 2 days following Her2 downregulation (-dox). At the time of Her2 downregulation, cells were treated with the pan-IKK inhibitor IKK16 (100 nM) or vehicle control. Results show the average of 3 biological replicates per condition.

Error bars denote mean \pm SEM. Significance was determined using a two-tailed Student's t-test.

Figure 1 – figure supplement 1 (a) qRT-PCR analysis of Erbb2 expression in primary cells with Her2 on (+dox) or Her2 off (-dox). (b) Gene set enrichment analysis (GSEA) of RNA-seq data showing an E2F gene signature is enriched in cells with Her2 signaling on. P-values and normalized enrichment scores (NES) are shown. (c) Western blot showing p65 phosphorylation in primary tumor cells treated with the indicated concentration of Neratinib for 24 hours, or 24 hours following dox withdrawal. (d-f) qRT-PCR analysis of TNF α , CCL5, and CXCL5 expression 24 hours after treatment with 0.1 μ M Neratinib. (g) qRT-PCR analysis of CCL2, CCL5, and CXCL5 expression in NIH-3T3 treated with 2 μ g/mL dox, 10 ng/mL TNF α , or both for 24 hours. (h) qRT-PCR analysis of Erbb2 expression of cells treated with -dox conditioned media with dox supplementation. (i) Primary tumor cells were treated with +dox conditioned media and activation of the NF- κ B pathway was assessed by Western blot analysis of total and phospho-p65. Results show 2 biological replicates per time point.

Figure 2) Immune cell infiltration during tumor regression and residual disease. (a) H&E-stained section of a representative residual tumor from a previously tumor-bearing MTB/TAN mouse. Insets show higher-magnification view of residual tumor cells (left) and staining for CK8 (right). (b-d) Representative images of a primary tumor (b), regressing tumor (5 days -dox) (c), and residual tumor (d), stained with H&E, Masson's Trichrome (MT), CD45, or F4/80. Primary tumors show little collagen deposition and only modest leukocyte infiltration. Her2 downregulation leads to infiltration of CD45+ cells, predominantly F4/80+ macrophages. Residual tumors have abundant collagen deposition and leukocyte infiltration.

Figure 2 – figure supplement 1) (a) CD3 staining of representative MTB;TAN primary, 5 days -dox, and residual tumors. (b) Bright-field and fluorescent images of a representative GFP-labeled orthotopic residual tumor in the context of a non-fluorescent mammary gland. (c) Quantification of IHC and MT staining of primary, regressing, and residual tumors from the MTB;TAN model. (d-f) F4/80 staining of representative orthotopic primary, 5 days -dox, and residual tumors showing macrophage infiltration.

Figure 3) Differential cytokine expression in residual tumors. (a) Volcano plot showing differential cytokine expression between primary and residual tumors. Antibody-based cytokine arrays were used to measure cytokine expression in orthotopic primary tumors or microdissected residual tumors. Cytokines that are upregulated (fold change >2, p-value <0.1) in dormant tumors are in red, and downregulated cytokines (fold change <-2, p-value <0.1) are in blue. Significance was determined using a two-tailed Student's t-test. (b) Quantification of CCL5, IL-13, IGFBP6, VCAM-1, OPG, HGF, Resistin, and P-Selectin expression in primary tumors and residual tumors. Values were derived from the cytokine arrays shown in (a). Significance was determined using a two-tailed Student's t-test. (c) CCL5 expression in 18 matched pre- and post-treatment samples from GSE10281. Red lines show tumors in which CCL5 expression increased following treatment (>1.5-fold change), and blue lines show tumors with decreased CCL5 expression (<1.5-fold change). (d) Average CCL5 expression in pre- and post-treatment samples from (c). Significance was determined using a two-tailed paired Student's t-test.

Error bars denote mean \pm SEM.

Figure 3 – figure supplement 1) (a) Heatmap showing expression of selected cytokine and chemokine genes from 18 matched human breast tumors prior to treatment, or in residual tumors following neoadjuvant Letrozole treatment (GSE10281). Gene expression values were log2 transformed and median centered. (b-m) Average expression of CCL2, CXCL1, CXCL2, CXCL5, SELE, HGF, IGFBP6, IL-13, TNFRSF11B, SELP, RETN, and VCAM-1 in 18 matched pre- and post-treatment samples following neoadjuvant Letrozole treatment (GSE10281). Two-tailed paired t-test was performed between pre- and post-treatment samples. (n) Average CCL5 expression in 25 matched pre- and post-treatment samples from human breast tumors treated with neoadjuvant chemotherapy (GSE21974). Two-tailed paired t-test was performed between pre- and post-treatment samples.

Figure 3 – source data) Cytokine array expression data analysis from arrays Q1 and Q4.

Figure 4) CCL5 expression promotes tumor recurrence following Her2 downregulation. (a) CCL5 protein levels in orthotopic primary (n=4), residual (n=3), and recurrent (n=2) tumors as determined by ELISA. **(b)** CCL5 protein levels in primary tumor cells engineered to express CCL5. Results show the mean \pm SEM for two independent experiments. Significance was determined using a two-tailed Student's t-test. **(c)** Recurrence-free survival for mice with control tumors or tumors expressing CCL5. CCL5 expression significantly accelerated recurrence (Hazards Ratio (HR) = 2.1, p = 0.02). Results are from a single experiment with 20 control tumors and 21 CCL5 tumors. P-values and hazards ratios are indicated. Statistical significance was determined by Mantel-Cox log rank test. **(d)** CCL5 expression as determined by ELISA in primary tumor cells expressing a control sgRNA or a sgRNA targeting CCL5. Results show the mean \pm

SEM for a single representative experiment. **(e)** Recurrence-free survival of mice with control tumors or CCL5 knockout tumors. CCL5 knockout in tumor cells did not significantly delay tumor recurrence (HR =0.76, $p = 0.46$). Results are from a single experiment with 26 control tumors (sgControl) and 24 sgCCL5 tumors. Statistical significance was determined by Mantel-Cox log rank test.

Error bars denote mean \pm SEM.

Figure 5) CCL5 promotes macrophage infiltration in residual tumors. (a-d) Flow cytometry of immune cells in primary (n=6), regressing (5 days -dox; n=3), residual (n=3), and recurrent (n=3) tumors from autochthonous MTB;TAN mice. Immune cell populations analyzed include CD11b+/F4/80+ macrophages (a), CD4+ T cells (b), CD8+ T cells (c), PDGFR α fibroblasts (d), and tumor cells (e). Each immune cell population was divided into CCR5- or CCR5+ cells, and the median fluorescence intensity (MFI) of the CCR5+ population was calculated. **(f)** Flow cytometry of CD45-/PDGFR α + fibroblasts in control residual tumors (n=4) or residual tumors expressing CCL5 (n=4). **(g)** Flow cytometry of CD11b+/F4/80+ macrophages in control residual tumors (n=4) or residual tumors expressing CCL5 (n=4).

Error bars denote mean \pm SEM. Significance was determined using a two-tailed Student's t-test. *

$p < 0.05$, ** $p < 0.01$, *** $p < 0.001$, **** $p < 0.0001$

Figure 5 - figure supplement 1) (a) qRT-PCR analysis of Erbb2 in primary, 5 days – dox, residual, and recurrent tumors from the MTB;TAN model cohort used for flow cytometry analysis

of CCR5 expression. (b) qRT-PCR analysis of CCR5 on sorted tumor cells and macrophages from primary, 5 days -dox, residual, and recurrent tumors from the MTB;TAN model. (c) Flow plots of CD45-/PDGFR α + fibroblasts in control (n=4) and CCL5-expressing (n=4) residual tumors (d) Flow plots of CD11b+/F4/80+ macrophages in control (n=4) and CCL5-expressing (n=4) residual tumors.

Figure 5 – figure supplement 2) Histograms showing CCR5 staining in macrophages, PDGFR α fibroblasts, CD4+ T cells, CD8+ T cells, and tumor cells from primary tumors (n=6), regressing tumors (5 days -dox; n=3), residual tumors (n=3), and recurrent tumors (n=3).

Figure 6) Macrophages express collagen and collagen deposition factors. (a) RNA-seq analysis of tumor associated macrophages from primary (n=3), regressing (5 days -dox; n=3), and recurrent (n=3) tumors. The heatmap shows differentially expressed genes ($p < 0.01$, Student's t-test) between primary and recurrent TAMs. (b) Heatmap showing expression of specific collagen genes from RNA-seq analysis in (a). (c) qRT-PCR analysis of COL5A1, ASPN, COL24A1, and PCOLCE expression in the cohort in (a) along with sorted macrophages from residual tumors. ND = not detected (d) qRT-PCR analysis of COL5A1, ASPN, COL24A1, and PCOLCE expression in unsorted MTB;TAN primary (n=5) and recurrent (n=5) tumors. (e) Masson's trichrome staining showing collagen deposition in primary (n=3), residual (n=3), and recurrent (n=3) tumors from the MTB;TAN model. Collagen is stained in blue, and higher collagen staining is present in residual and recurrent tumors. (f) Masson's trichrome staining in a subset of control and CCL5-expressing orthotopic recurrent tumors. The entire cohort of tumors is shown in Figure 6 – figure supplement 1.

800

801 Error bars denote mean \pm SEM. Significance was determined using a two-tailed Student's t-test. *

802 $p < 0.05$, *** $p < 0.001$.

803

804 **Figure 6 – figure supplement 1)** (a) Average expression of ASPN, COL5A1, COL24A1, and
 805 PCOLCE in 18 matched pre- and post-treatment samples from human breast tumors treated with
 806 neoadjuvant Letrozole (GSE10281). Two-tailed paired t-test was performed between pre- and
 807 post-treatment samples. (b) Masson's trichrome staining showing collagen deposition in control
 808 (n=4) and CCL5-expressing (n=4) recurrent tumors. (c) Quantification of (b).

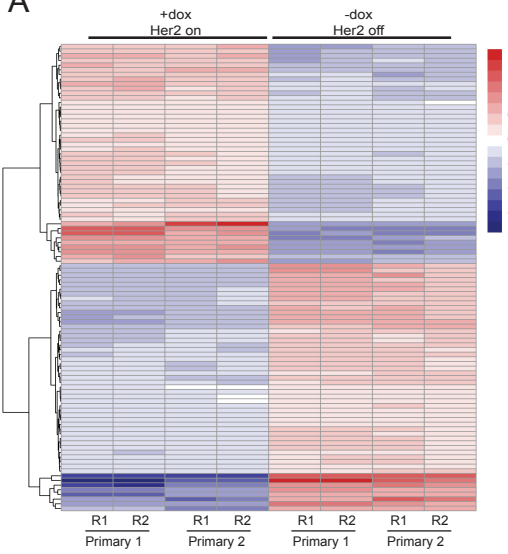
809

810 **Figure 6 – source data 1)** Differentially expressed genes from RNA-seq from primary and
 811 recurrent tumor cell lines used to clear contaminants from TAM RNA-seq

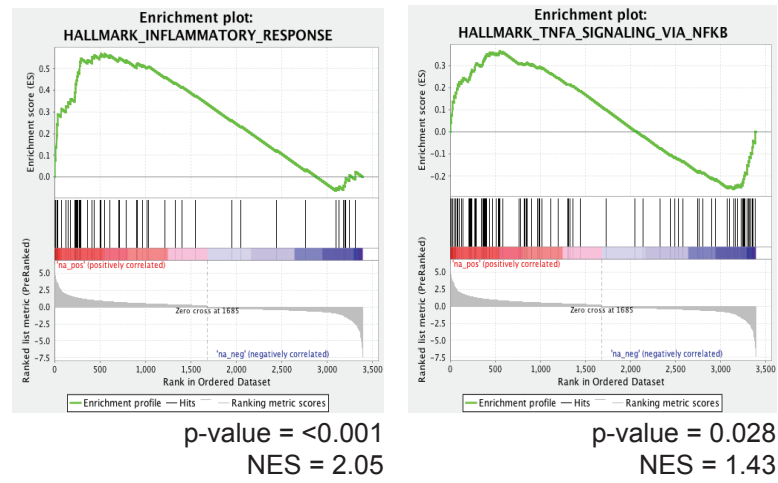
812 **Figure 6 – source data 2)** Candidate list of differentially expressed genes between primary and
 813 recurrent TAMs after filtering

814

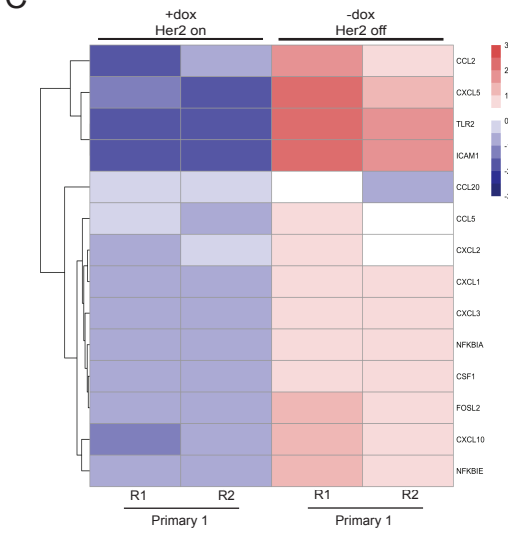
A



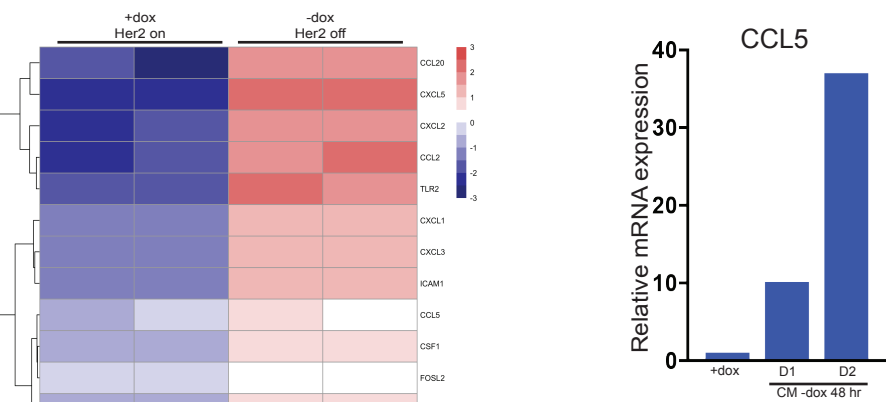
B



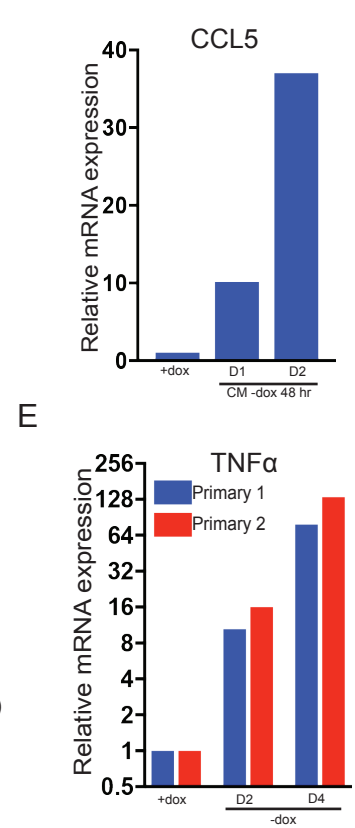
C



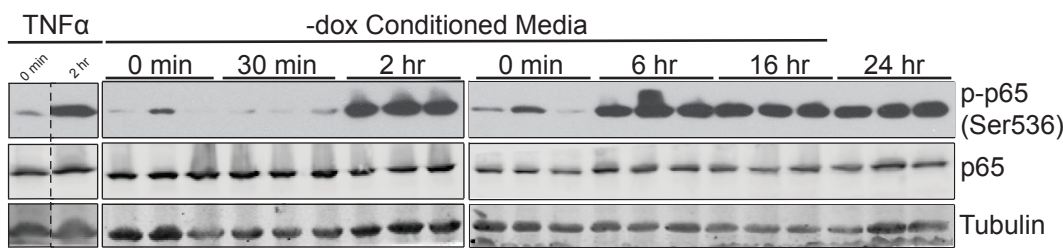
D



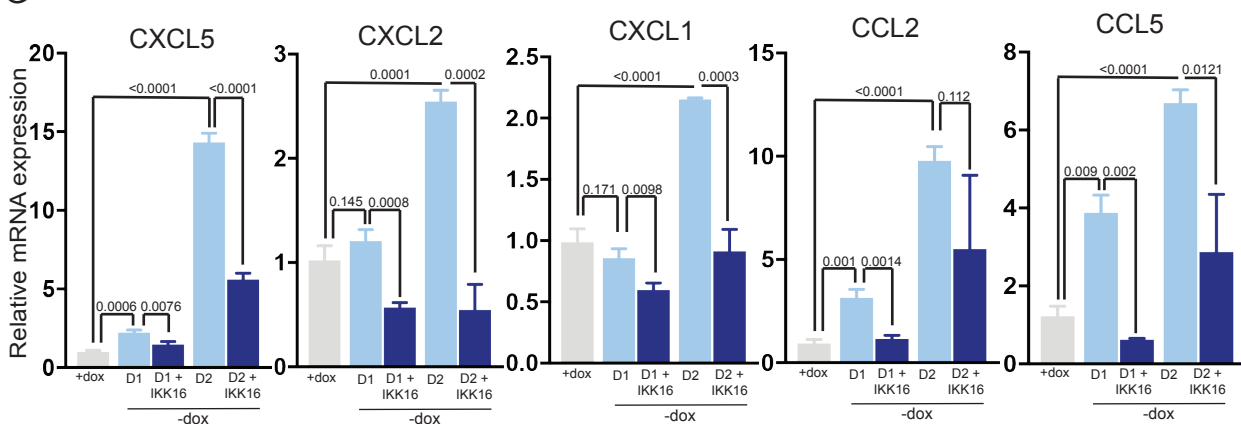
E

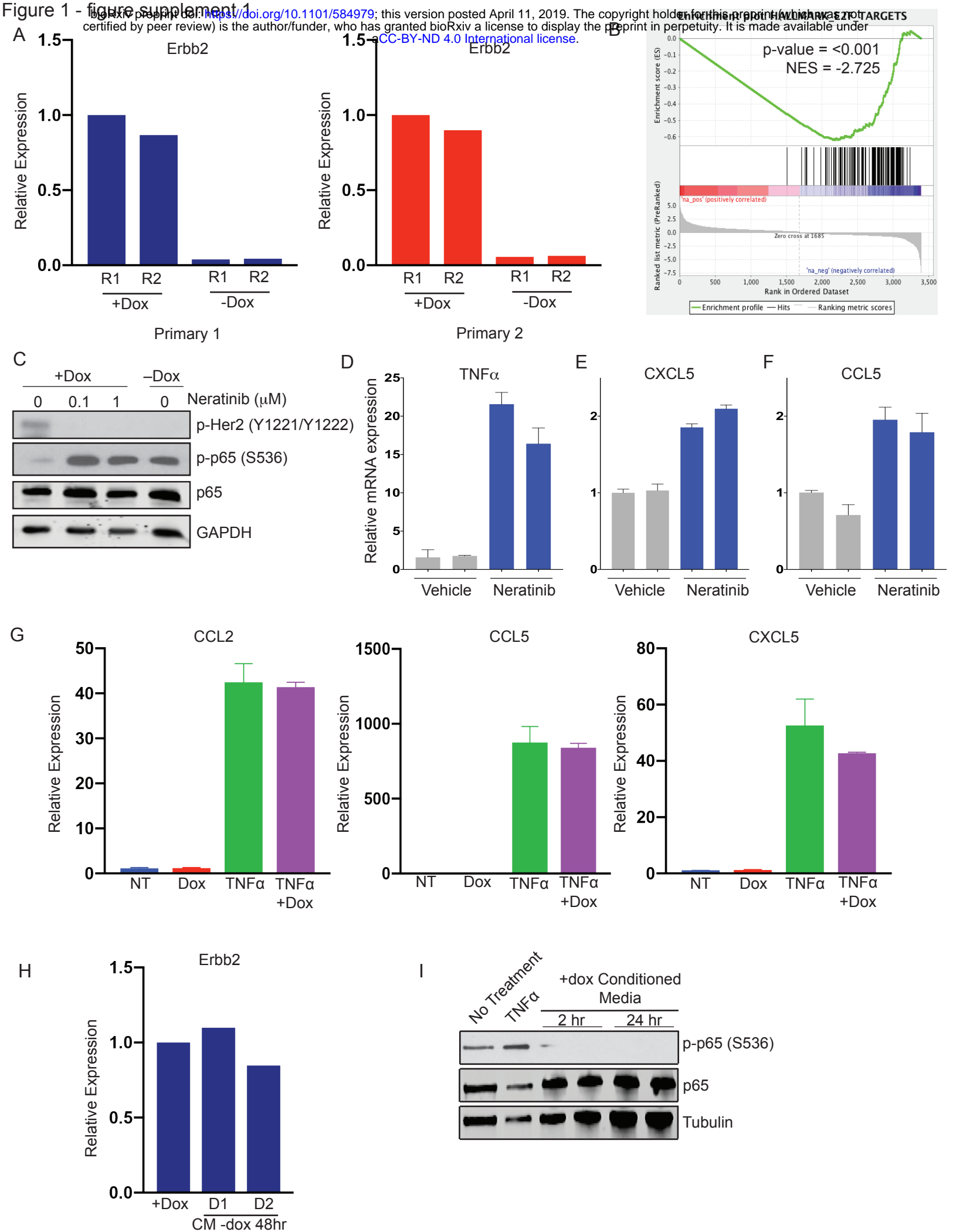


F

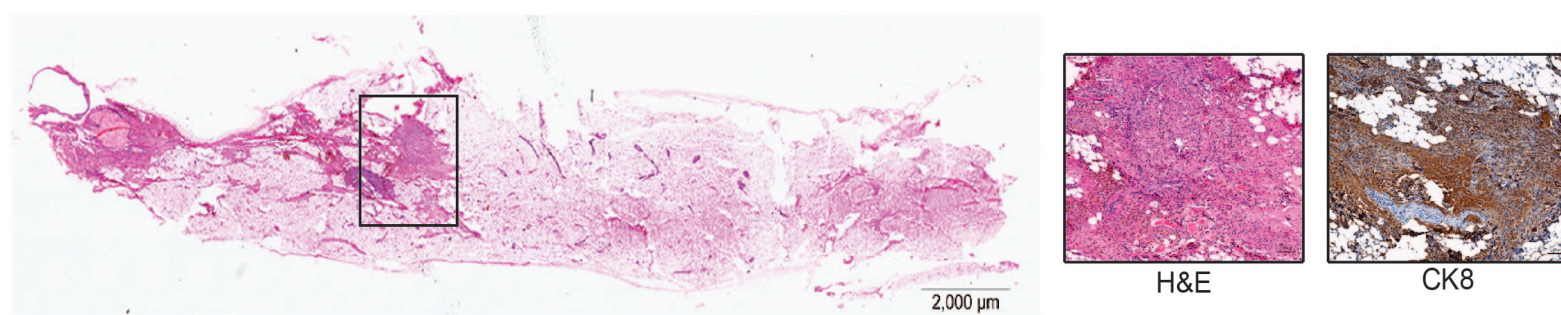


G



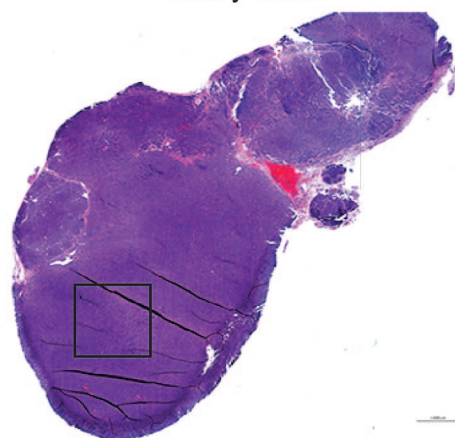


A



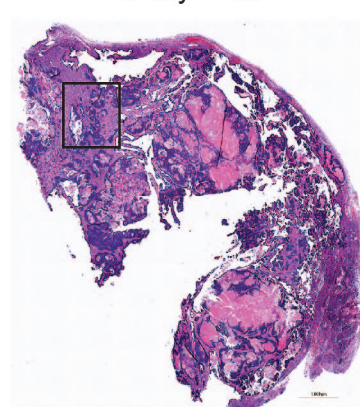
B

Primary Tumor



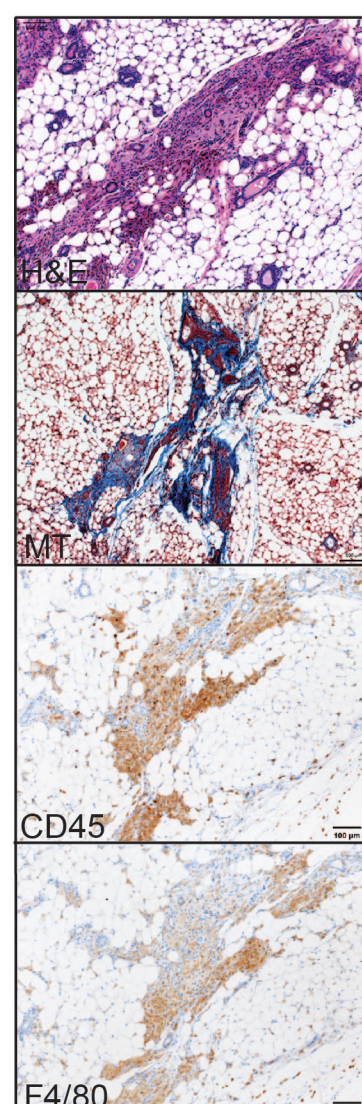
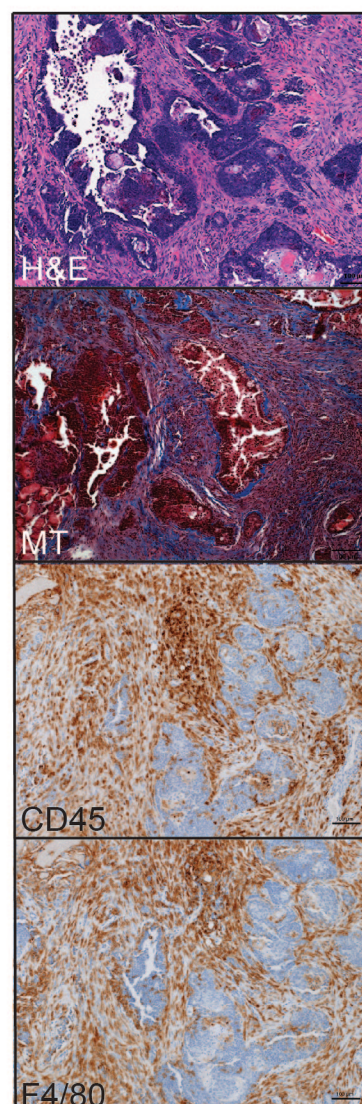
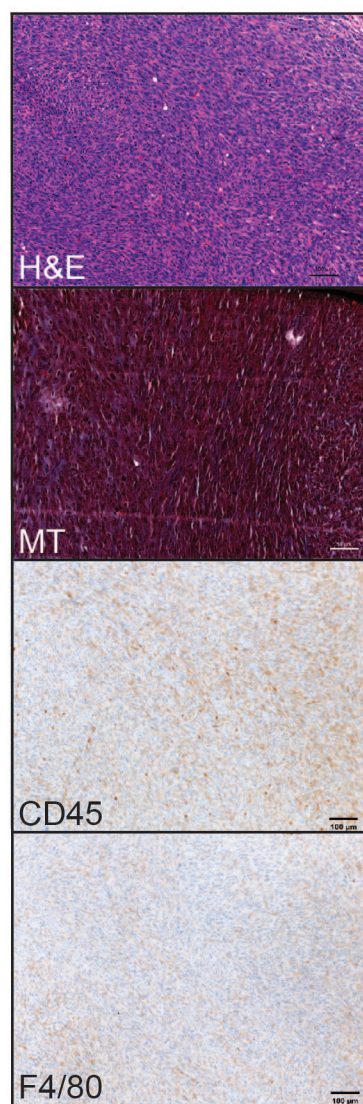
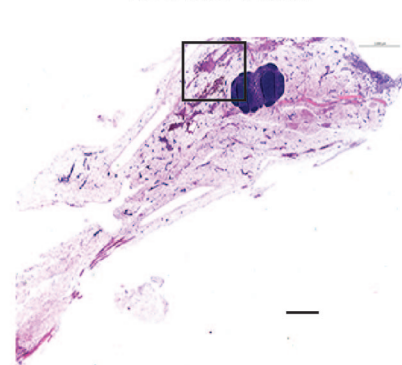
C

5 day -Dox

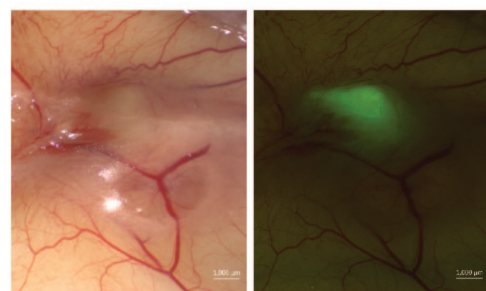
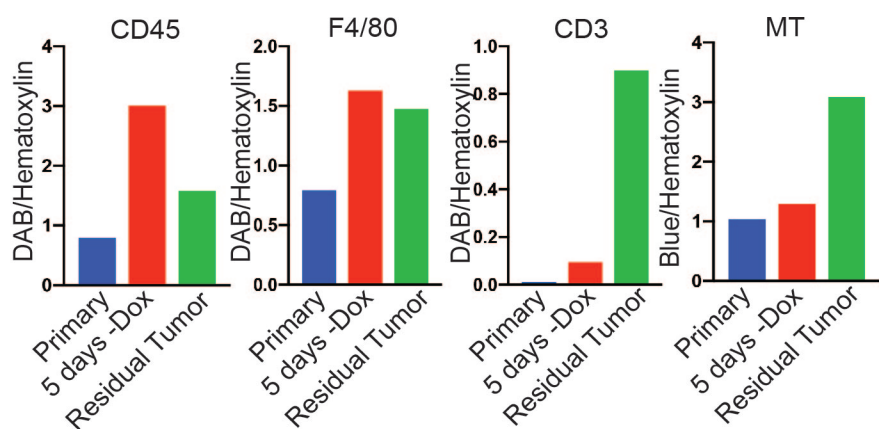


D

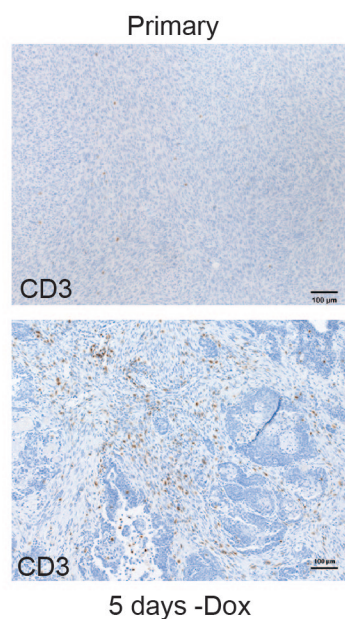
Residual Tumor



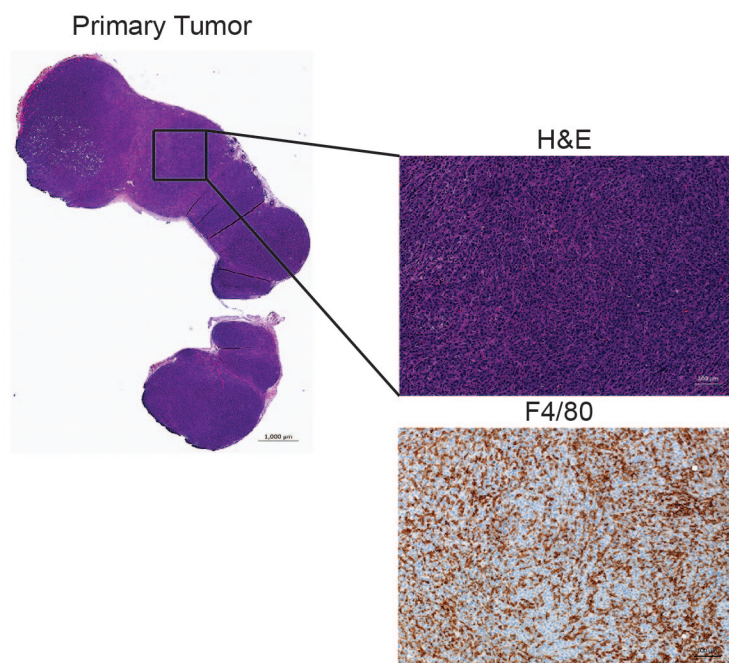
A



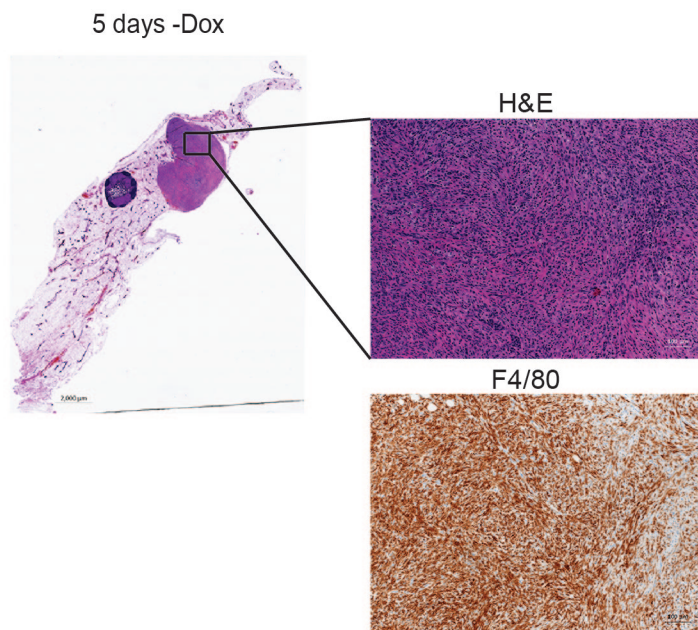
B



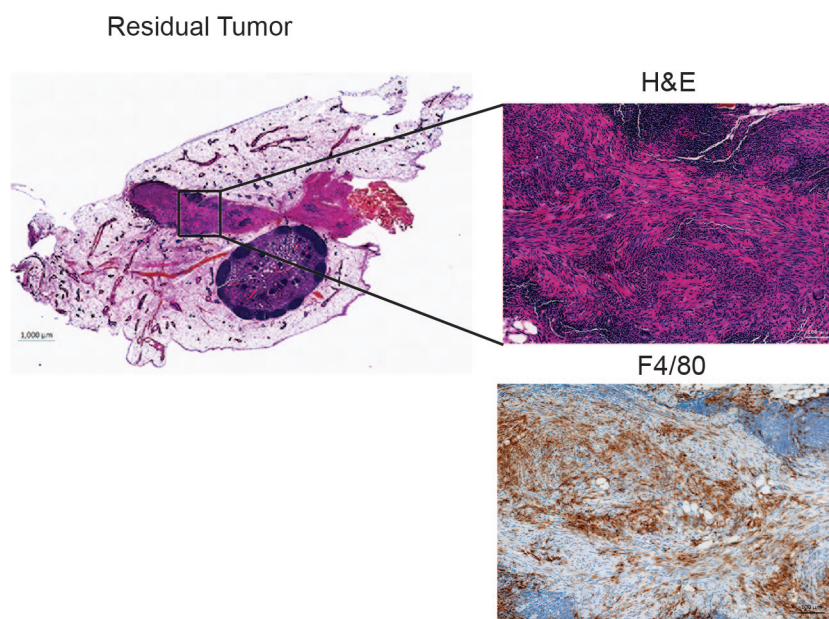
D



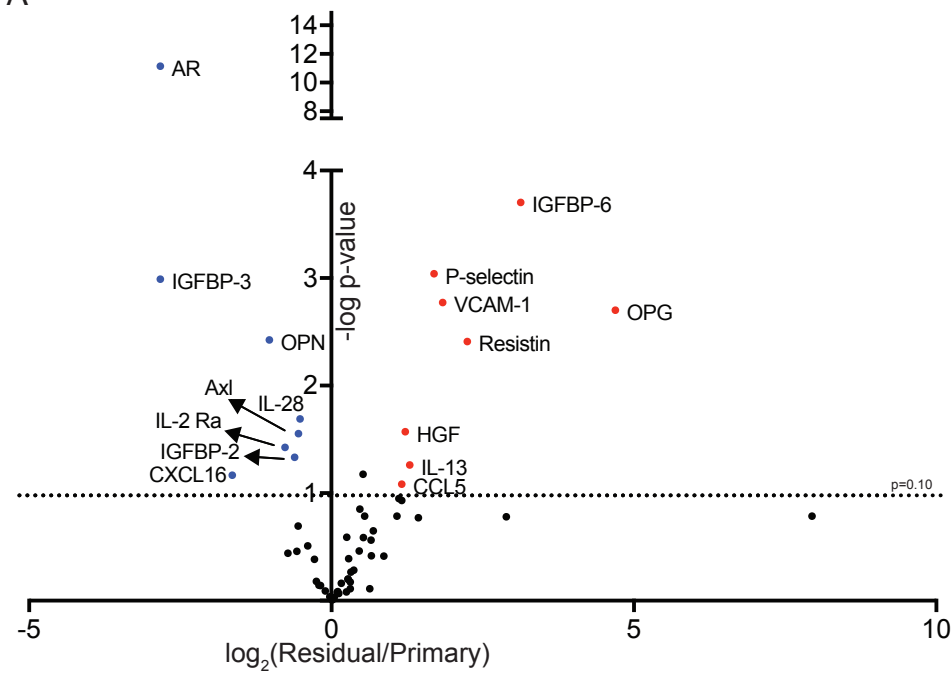
E



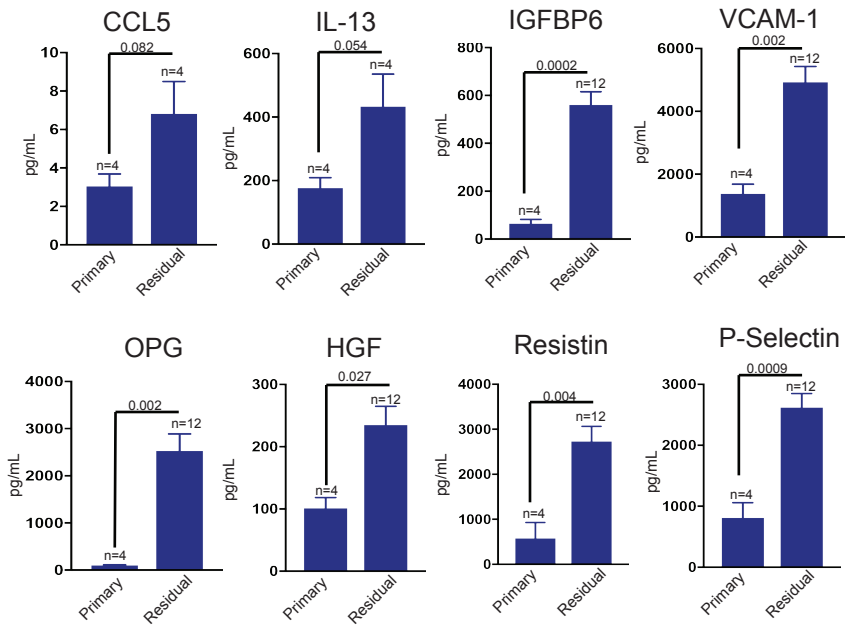
F



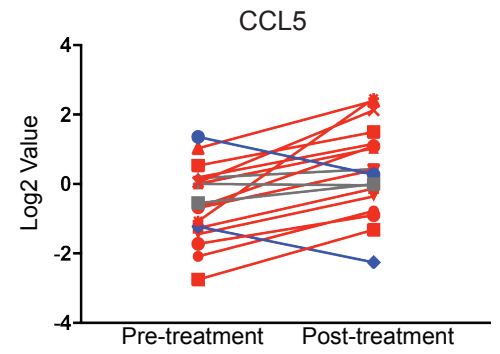
A



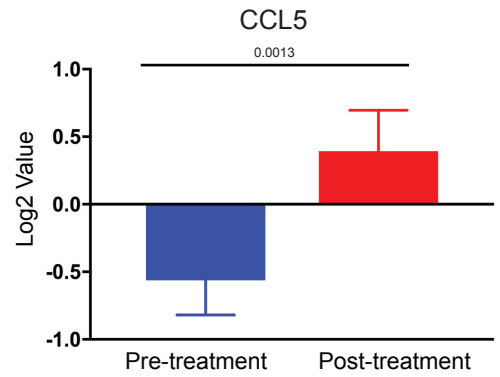
B

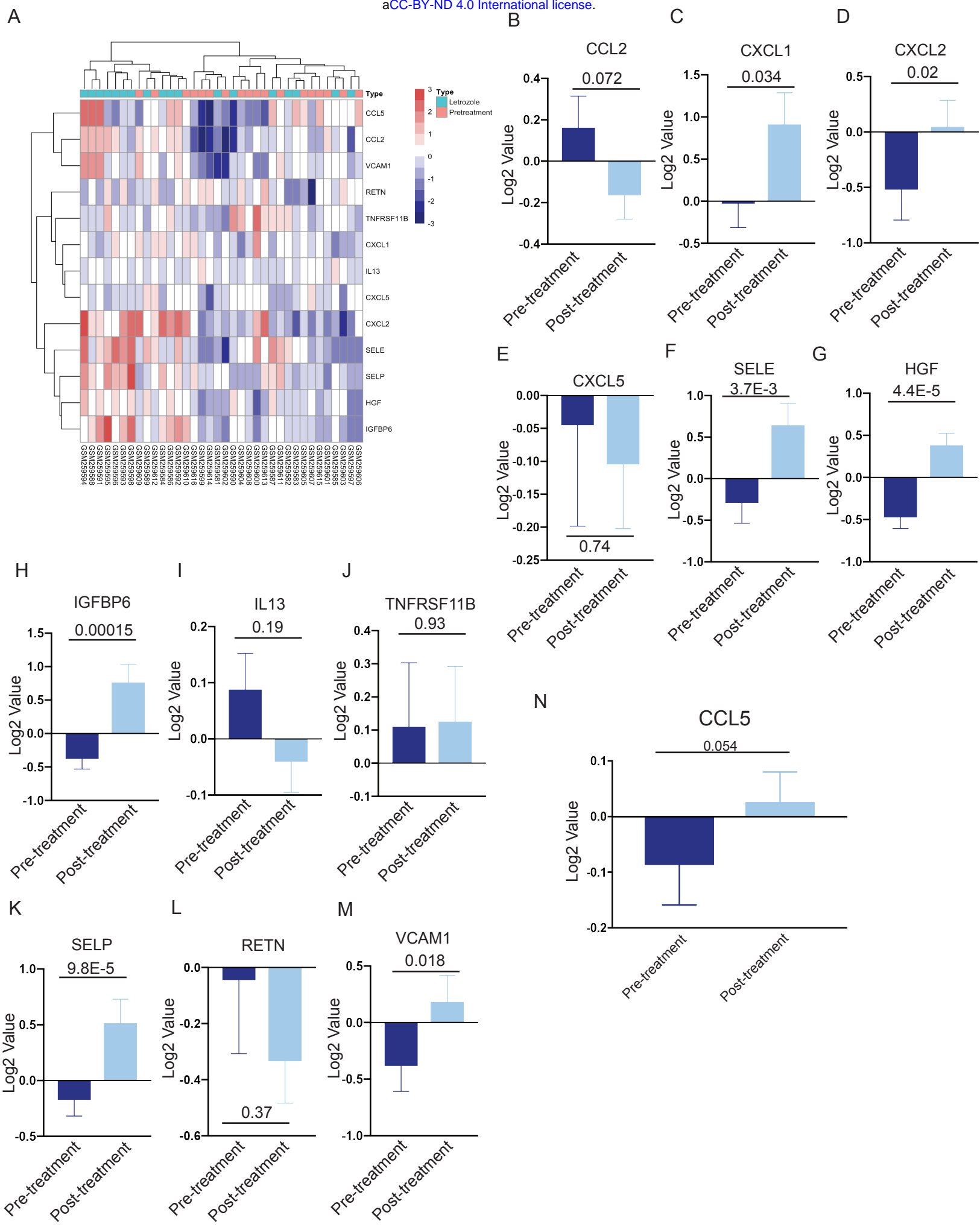


C



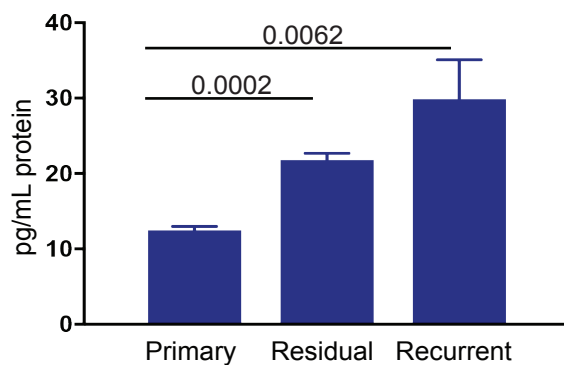
D





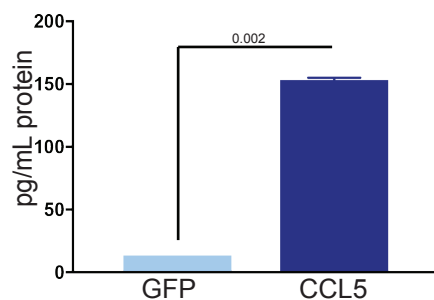
A

CCL5

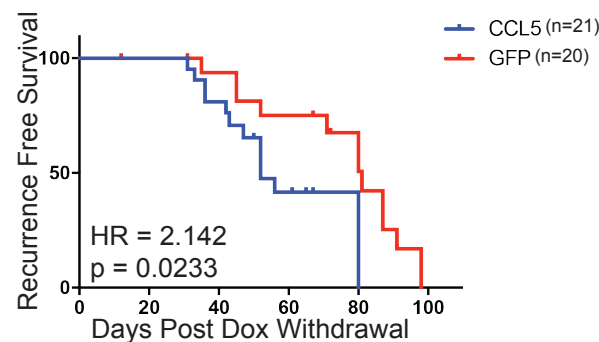


B

CCL5

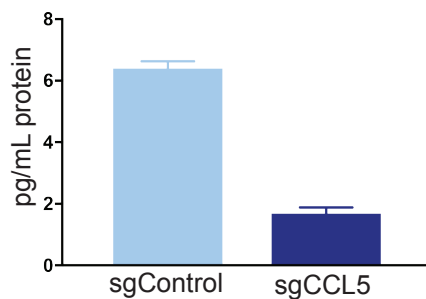


C

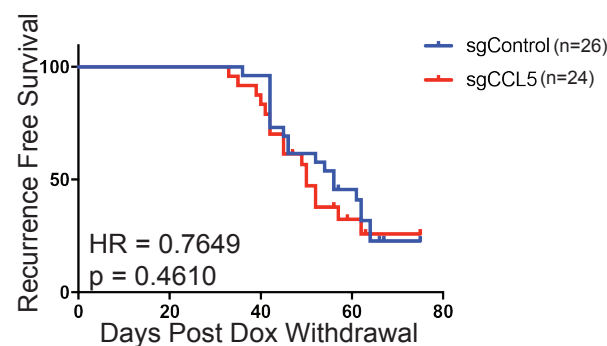


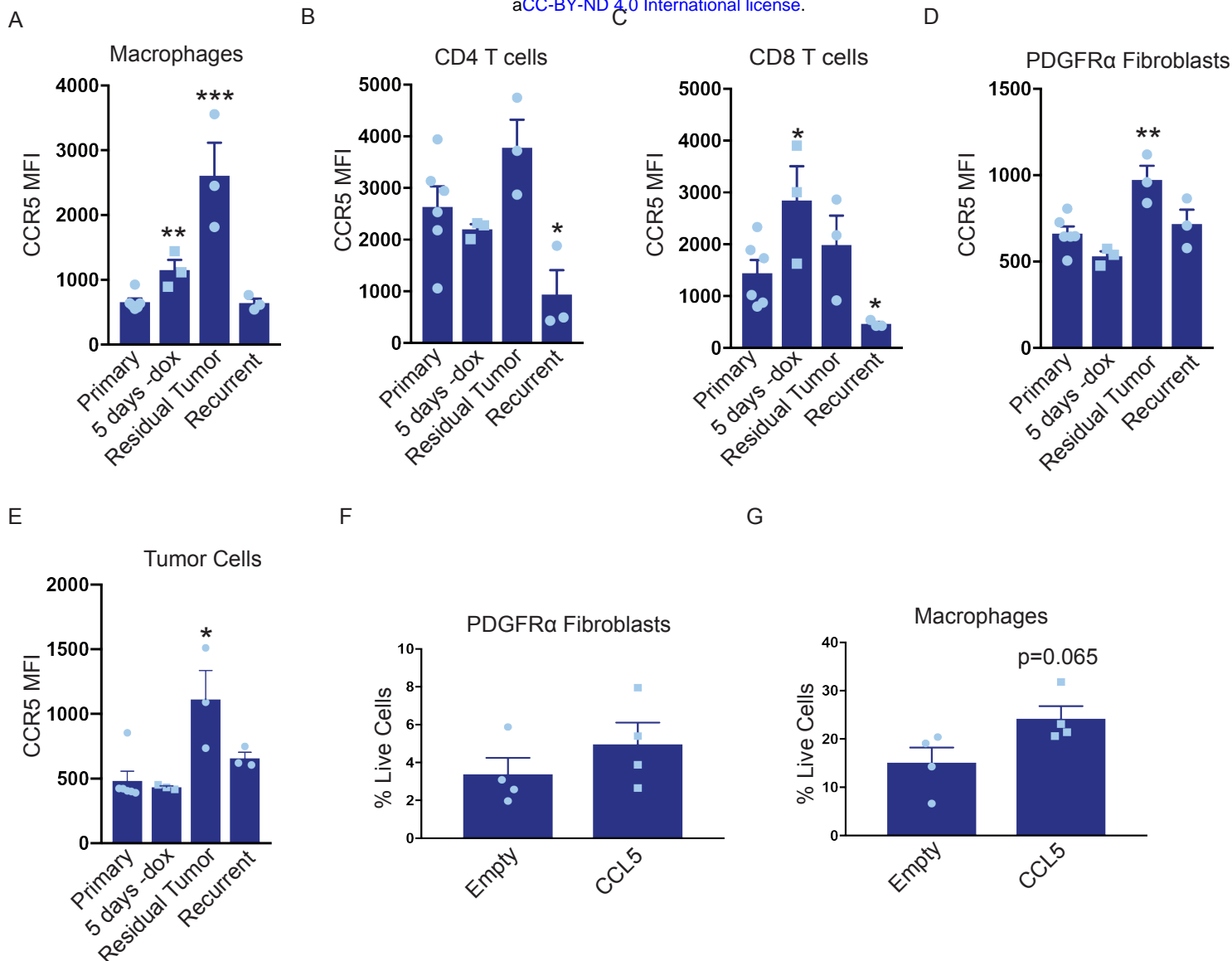
D

CCL5

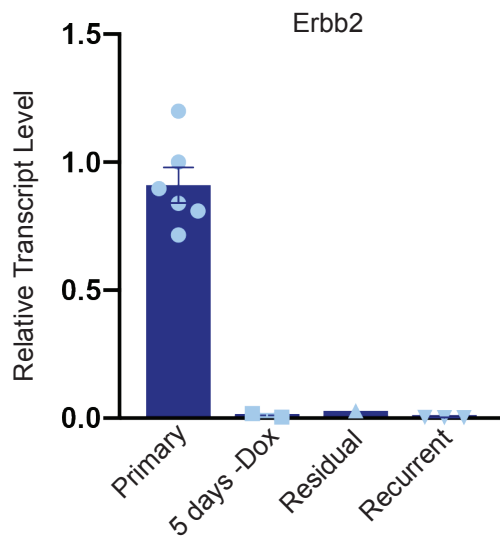


E

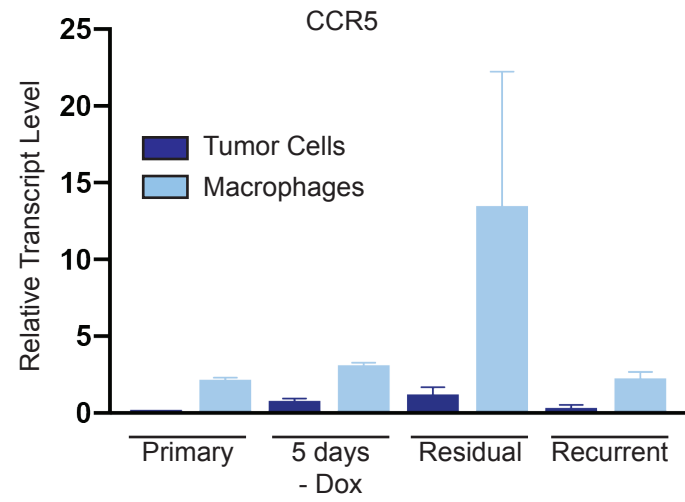




A

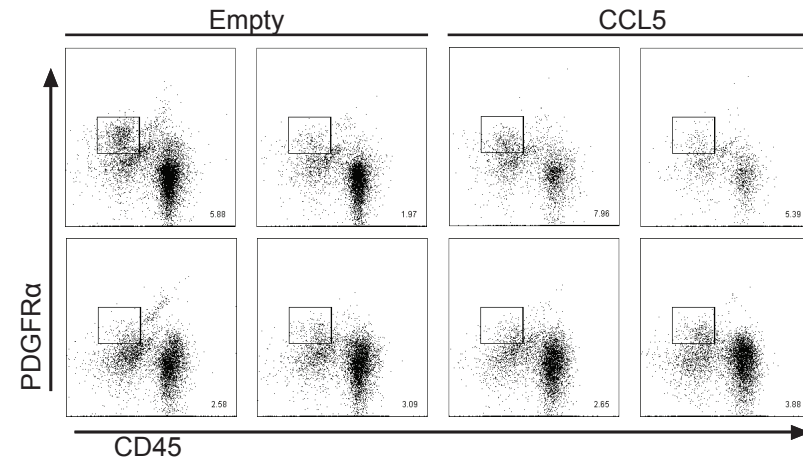


B



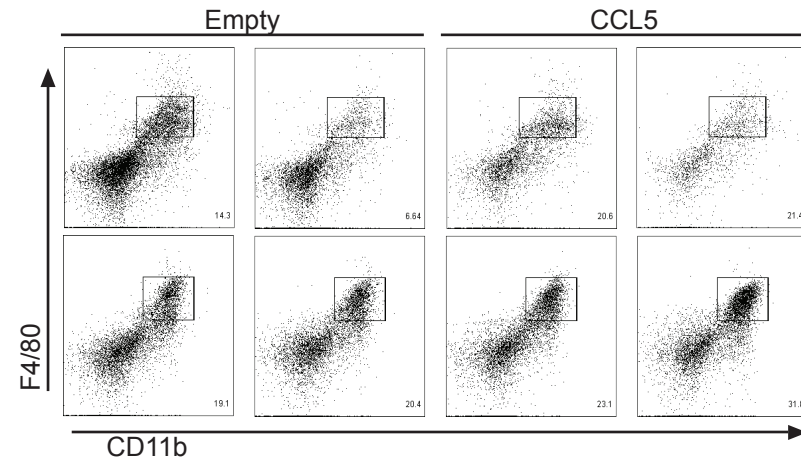
C

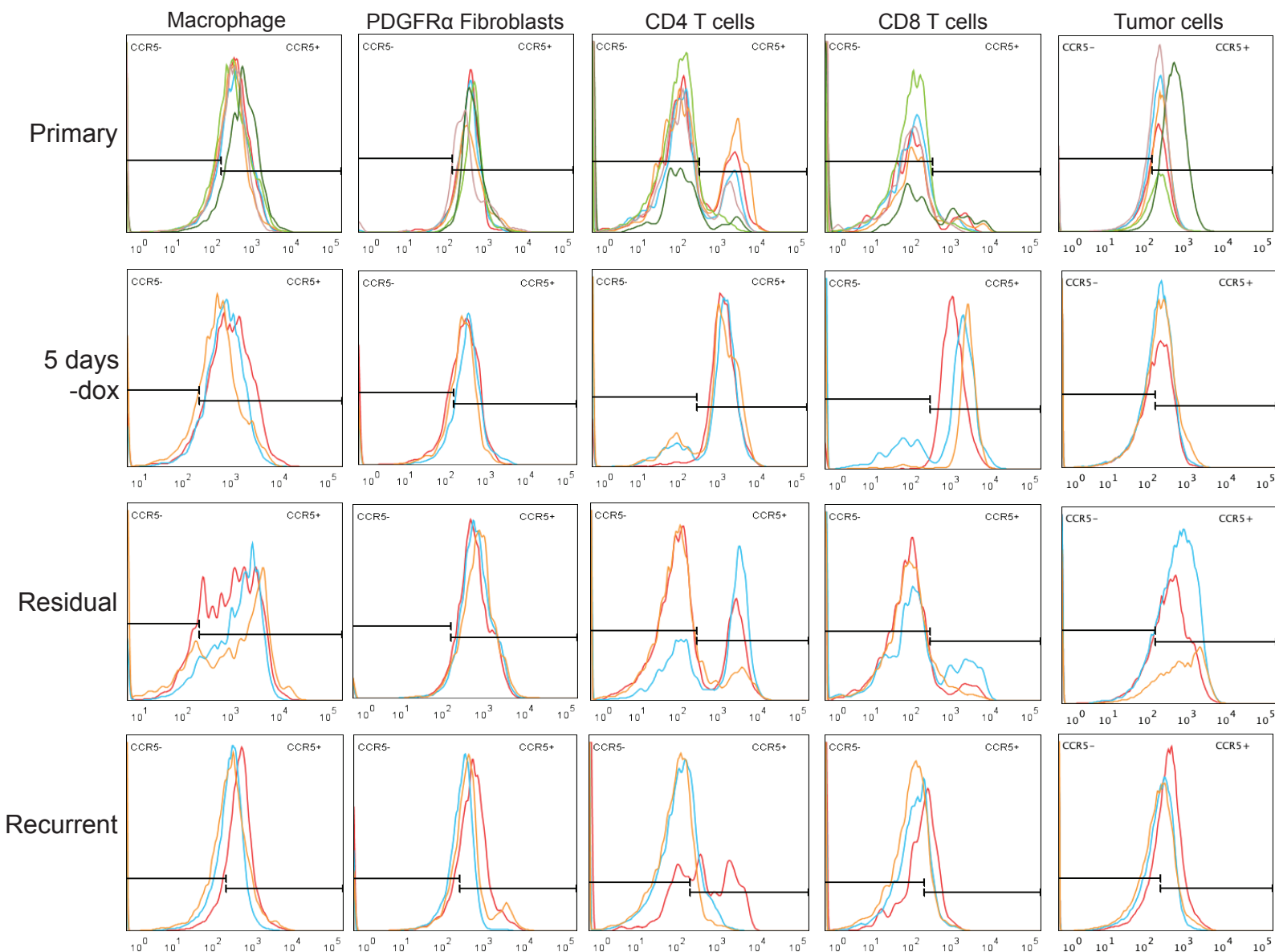
PDGFR α Fibroblasts

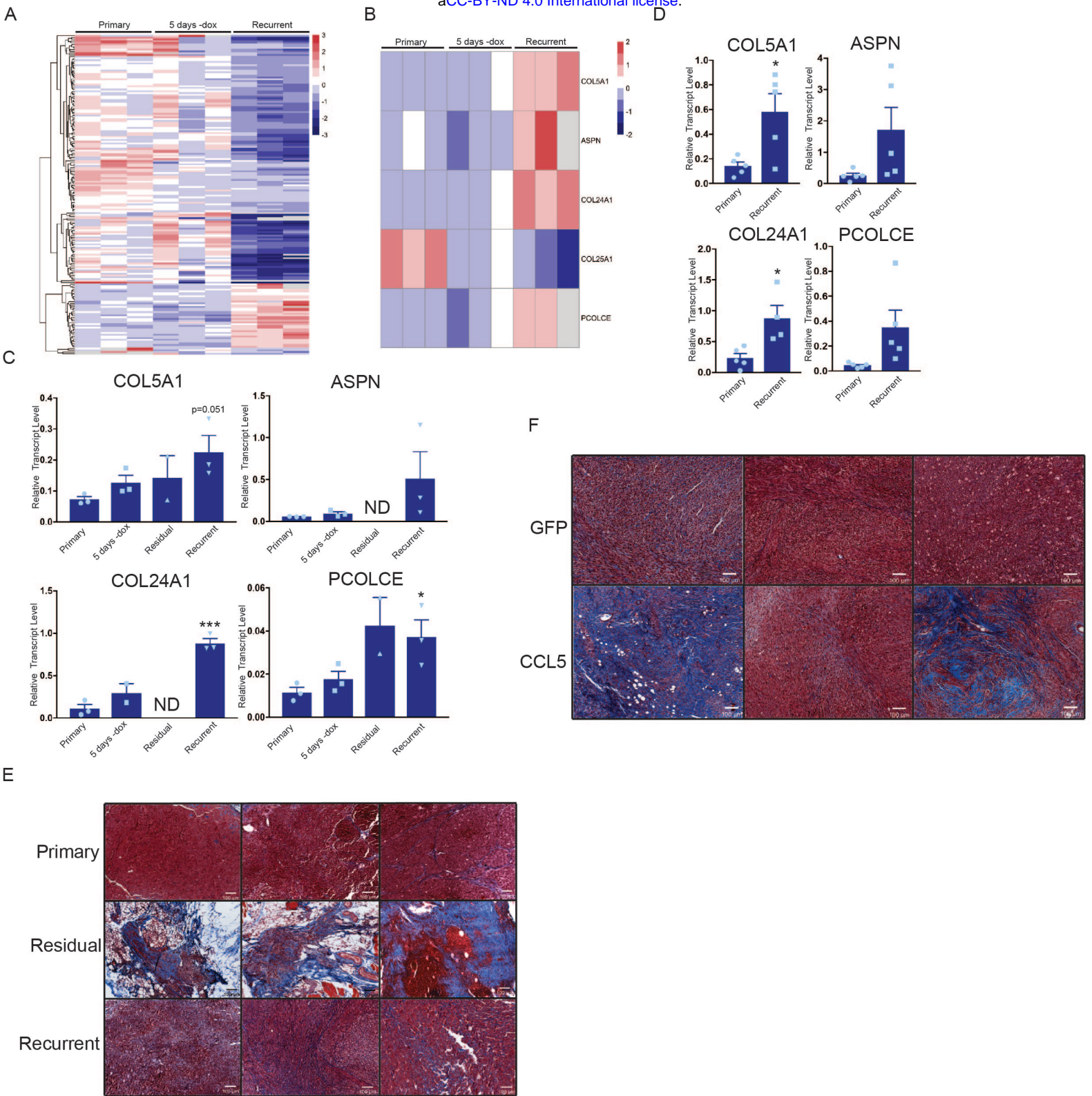


D

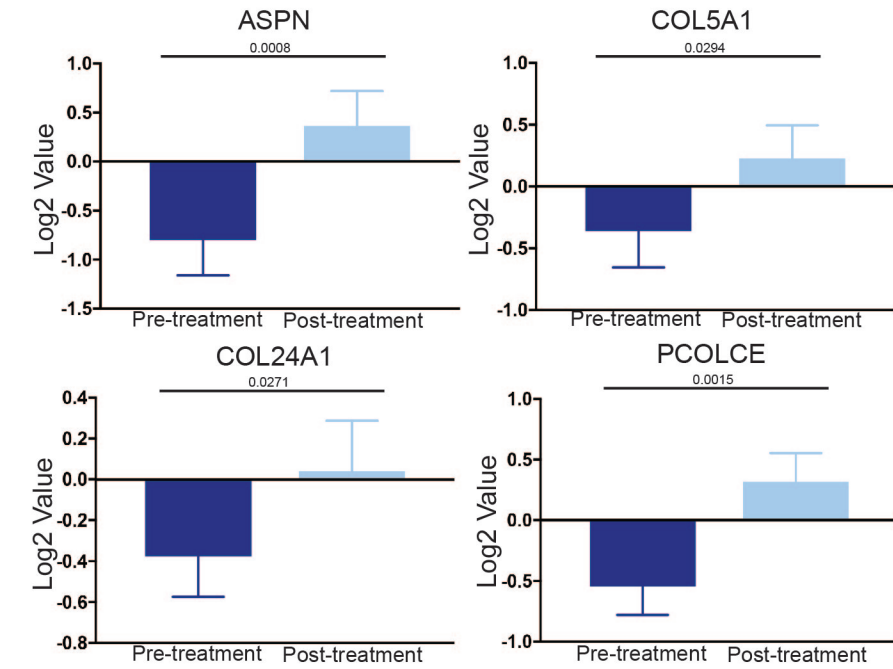
Macrophage



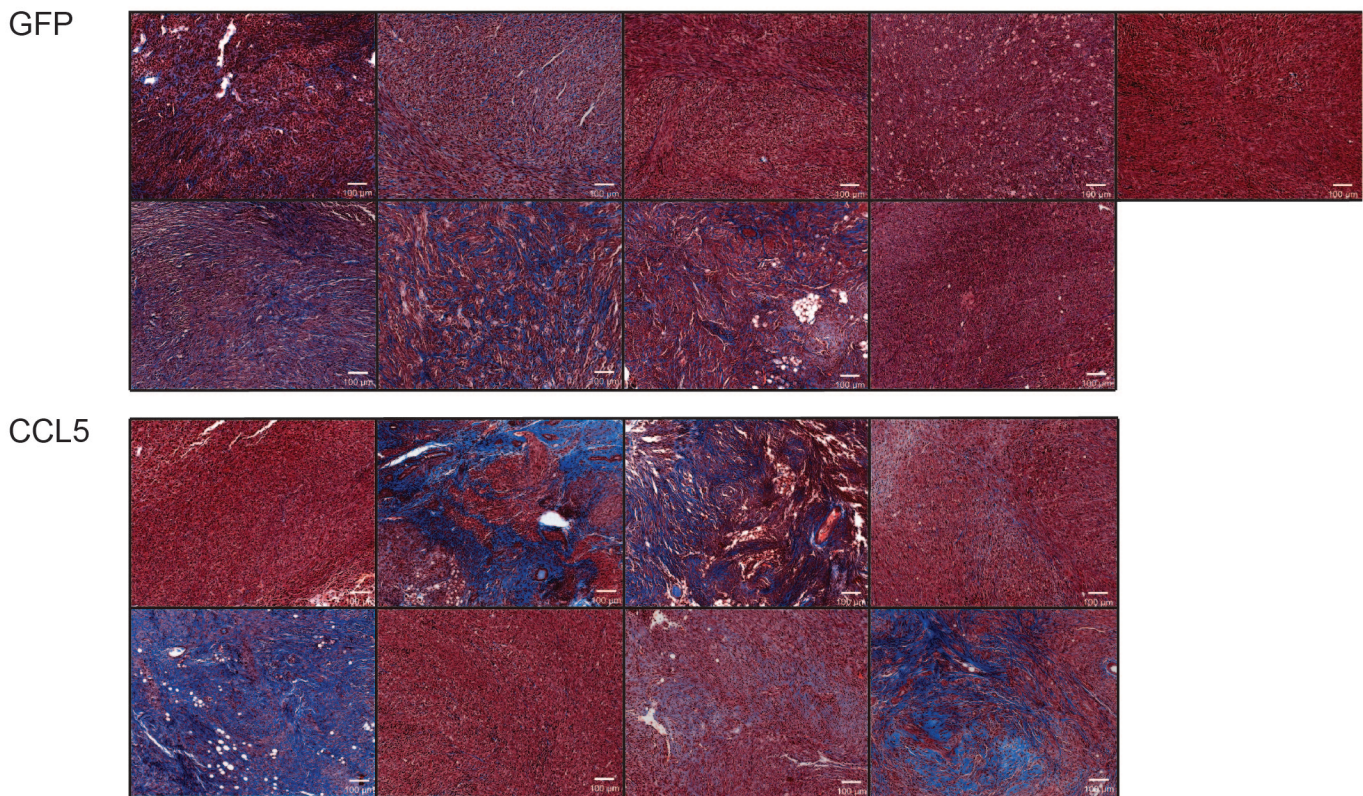




A



B



C

